JEM Journal of Experimental Medicine

ARTICLE

Sleep exerts lasting effects on hematopoietic stem cell function and diversity

Cameron S. McAlpine[1,2,3*], Máté G. Kiss[1,3*], Faris M. Zuraikat[4,8], David Cheek[3], Giulia Schiroli[5,6], Hajera Amatullah[7], Pacific Huynh[1], Mehreen Z. Bhatti[8], Lai-Ping Wong[9], Abi G. Yates[1], Wolfram C. Poller[1,3], John E. Mindur[3], Christopher T. Chan[1,3], Henrike Janssen[1,3], Jeffrey Downey[1,3], Sumnima Singh[1,3], Ruslan I. Sadreyev[9,10], Matthias Nahrendorf[3], Kate L. Jeffrey[7], David T. Scadden[5,6], Kamila Naxerova[3], Marie-Pierre St-Onge[4,8], and Filip K. Swirski[1,3]

A sleepless night may feel awful in its aftermath, but sleep's revitalizing powers are substantial, perpetuating the idea that convalescent sleep is a consequence-free physiological reset. Although recent studies have shown that catch-up sleep insufficiently neutralizes the negative effects of sleep debt, the mechanisms that control prolonged effects of sleep disruption are not understood. Here, we show that sleep interruption restructures the epigenome of hematopoietic stem and progenitor cells (HSPCs) and increases their proliferation, thus reducing hematopoietic clonal diversity through accelerated genetic drift. Sleep fragmentation exerts a lasting influence on the HSPC epigenome, skewing commitment toward a myeloid fate and priming cells for exaggerated inflammatory bursts. Combining hematopoietic clonal tracking with mathematical modeling, we infer that sleep preserves clonal diversity by limiting neutral drift. In humans, sleep restriction alters the HSPC epigenome and activates hematopoiesis. These findings show that sleep slows decay of the hematopoietic system by calibrating the hematopoietic epigenome, constraining inflammatory output, and maintaining clonal diversity.

Introduction

Sleep profoundly influences immune and inflammatory responses, protecting against age-associated immune disorders including cardiovascular disease (CVD), cancer, and neurodegenerative diseases (Besedovsky et al., 2019; Irwin, 2019). Despite these associations, more than half of adults do not get sufficient sleep (Ford et al., 2015; Langer and Filer, 2020). Sleep impacts many facets of the immune system including adaptive responses, inflammation, and the synthesis of cytokines and immune mediators (Dimitrov et al., 2004; Lange et al., 2006; Irwin, 2019). Yet, the influence of sleep on hematopoietic stem and progenitor cells (HSPCs) and immune cell production is poorly understood. In humans, poor quality sleep and sleep disorders are associated with increased blood myeloid cells (Ruiz et al., 2012; Geovanini et al., 2018; Vallat et al., 2020), and in murine models, sufficient sleep restricts leukocytosis by limiting HSPC cycling in the bone marrow (BM) through neuroimmune mechanisms (McAlpine et al., 2019). In human and murine atherosclerotic CVD, prolonged sufficient sleep reduces the number of blood monocytes and neutrophils, constraining leukocyte infiltration into the arterial wall and reducing lesion size (McAlpine et al., 2019; Vallat et al., 2020). It has remained unclear, however, how sleep might influence HSPC programming and function.

Sleep abundance and quality vary over an individual's lifespan (Ohayon et al., 2004; Kamel and Gammack, 2006), and the impact of sleep variability on long-term immune-related outcomes is unclear. Sleep declines with age (Unruh et al., 2008), and even young healthy adults are prone to vacillations between periods of adequate and insufficient sleep (Lallukka et al., 2012; Ferguson et al., 2021), which can be shaped by genetically imprinted chronotypes and altered by lifestyle and environments. Bouts of suboptimal sleep, even if followed by periods of

[1]Cardiovascular Research Institute and the Department of Medicine, Cardiology, Icahn School of Medicine at Mount Sinai, New York, NY; [2]Friedman Brain Institute and the Nash Family Department of Neuroscience, Icahn School of Medicine at Mount Sinai, New York, NY; [3]Center for Systems Biology and the Department of Radiology, Massachusetts General Hospital and Harvard Medical School, Boston, MA; [4]Sleep Center of Excellence, Department of Medicine, Columbia University Irving Medical Center, New York, NY; [5]Center for Regenerative Medicine, Massachusetts General Hospital, Boston, MA; [6]Department of Stem Cell and Regenerative Biology, Harvard Stem Cell Institute, Harvard University, Cambridge, MA; [7]Division of Gastroenterology and Center for the Study of Inflammatory Bowel Disease, Department of Medicine, Massachusetts General Hospital and Harvard Medical School, Boston, MA; [8]Division of General Medicine, Department of Medicine, Columbia University Irving Medical Center, New York, NY; [9]Department of Molecular Biology, Massachusetts General Hospital and Department of Genetics, Harvard Medical School, Boston, MA; [10]Department of Pathology, Massachusetts General Hospital and Harvard Medical School, Boston, MA.

*C.S. McAlpine and M.G. Kiss contributed equally to this paper. Correspondence to Filip K. Swirski: filip.swirski@mssm.edu; Marie-Pierre St-Onge: ms2554@cumc.columbia.edu; Cameron S. McAlpine: cameron.mcalpine@mssm.edu.

sufficient sleep, may have adverse health effects, and recent studies using large human cohorts have indicated that so-called "catch-up" sleep is insufficient at reversing or even neutralizing the adverse effects of sleep debt (Depner et al., 2019; Leger et al., 2020; Dashti et al., 2021). Despite these observations, the impact of sleep and oscillations in sleep quality on future immune function and disease susceptibility are poorly understood, yet critical to uncovering the links between sleep and chronic immune and inflammatory diseases that develop over decades. In this study, we explored how sleep fragmentation (SF) and its recovery shape immunological responses and disease outcomes through epigenetic restructuring of HSPCs. We assess the impact of SF on the clonal diversity of immune cells and the genetic aging of the hematopoietic system. To expand our analysis, we quantify hematopoiesis and HSPC programming in humans participating in a sleep restriction (SR) trial.

Results

Sleep exerts a prolonged influence on hematopoiesis

To explore how sleep might influence prolonged immune function, we first subjected mice to mechanical SF, tactilely rousing mice every 2 min during their rest period (Zeitgeber [ZT] 0–12; McAlpine et al., 2019). We recorded electroencephalography (EEG) signals from the brain and electromyography (EMG) signals from muscle to quantify sleep and wake states and transitions. As expected, SF increased the number of wake bouts (transitions from sleep to wake states) during the rest period (Fig. 1 A). SF did not alter slow wave sleep (SWS), rapid eye movement sleep (REM), or wake time during the light period (Fig. 1 B). However, SWS was increased and wake time was reduced during the first 2 h of their active period (ZT13 and 14). We next tested whether fragmented sleep was maintained during long exposures to SF and if it reverts after terminating tactile disruption. We subjected mice to 16 wk of SF followed by 10 wk of undisturbed sleep (recovery sleep [RS]) while continuously monitoring EEG and EMG signals. Wake bouts remained elevated throughout the entire 16 wk of SF (Fig. 1 C). During RS, wake bouts were elevated for the first 2 wk before returning to baseline for the remaining 8 wk (Fig. 1 C). Together, these findings suggest a lasting if not a permanent influence of SF on sleep quality.

In mice, 16 wk of SF augments hematopoiesis and the proliferation of lineage$^-$Sca1$^+$cKit$^+$ (LSK) cells in the BM, leading to an increased number of blood Ly6C^{hi} monocytes during the rest period (McAlpine et al., 2019). In the BM, SF increases the concentration of myeloid colony–stimulating factor (M-CSF; McAlpine et al., 2019) but does not alter kit ligand, IL-3, or GM-CSF (Fig. S1, A and B). In the plasma, SF raises IL-6 levels while other plasma cytokines, growth factors, corticosterone, and body weight remain unchanged (Fig. S1, C and D). Considering our data on wake bouts during RS, we sought to determine how long increased leukocyte production persists in mice allowed to recover from 16 wk of SF. After 4 wk of RS, at ZT3, blood Ly6C^{hi} monocytes, BM LSKs, and LSK proliferation remained elevated relative to control mice having slept habitually (Fig. 1 D). However, after 10 wk of RS in a separate cohort of animals, hematopoietic activity, monocytosis, and IL-6 levels receded to control levels (Fig. 1 E and Fig. S1 G). Relative to control mice, measured plasma and BM cytokines and growth factors, plasma corticosterone, and body weight remained unaltered after 10 wk of RS (Fig. S1, E–H). Enhanced hematopoietic activity, therefore, persists for weeks after cessation of SF, raising the possibility that SF exerts a lasting, if not permanent, influence on leukocyte production. To begin to explore this hypothesis, we performed competitive LSK transplantation assays. We transplanted LSKs at a 1:1 ratio from SF (CD45.2) and control (CD45.1) mice into irradiated GFP mice and allowed recipient mice to sleep habitually. 3 wk after transplantation, we measured the proliferation of LSKs derived from SF (GFP$^-$CD45.2$^+$) and control (GFP$^-$CD45.1$^+$) animals. Despite similar initial engraftment (Fig. S1 I) and inhabiting the same BM microenvironment, LSKs of SF mice incorporated more BrdU than controls (Fig. 1 F). To extend this observation, we tracked CD45.1/2 chimerism in the blood up to 24 wk after transplant. Cells arising from SF mice outcompeted cells from control mice and comprised >60% of the leukocyte and monocyte fractions in the blood (Fig. 1 G). We made similar observations when LSKs from CD45.2 SF mice were placed in competition with LSKs from UBI-GFP mice (CD45.2) sleeping habitually (Fig. S1 J). Combined, these findings point to stem-intrinsic mechanisms that regulate prolonged SF-mediated hematopoietic activity.

Sleep programs the epigenome of hematopoietic progenitor cells and instructs adaptability

To test stem-intrinsic mechanisms of sleep-mediated hematopoiesis, we profiled the epigenome of hematopoietic progenitor cells in the BM. First, we observed increased histone deacetylase (HDAC) activity in hematopoietic progenitor cells of SF mice (Fig. S1 K). Next, we performed the assay for transposase-accessible chromatin sequencing (ATAC-seq) on LSKs sorted from three groups of mice: control mice (habitual sleep [HS]), mice subjected to 16 wk of SF, and mice subjected to 16 wk of SF, followed by 10 wk of RS (Fig. 2 A), a time point when LSK number and proliferation have receded (Fig. 1 E). Though we found ATAC-seq peaks distributed throughout the genome (Fig. S1 L), we focused our attention on peaks mapping to enhancer elements, which are regions critical to gene expression. Relative to controls, 470 enhancer loci were differentially accessible (DA) in LSKs of SF mice (vs. controls, 65 gained accessibility and 405 lost accessibility, $Log_2FC > 2$, $P < 0.05$, Fig. 2, B and C), revealing broad reprogramming of the epigenome by SF. Next, we compared peaks common to all three groups. We found that 69% (319) of the SF-induced changes in enhancer accessibility reverted to control levels after 10 wk of RS. However, 31% (140 loci) of alterations caused by SF were maintained in the RS group, representing a preserved signature and a potential mark of sustained epigenetic imprinting (Fig. 2 C). Pathway analysis of the preserved signature uncovered elements of cell cycle and cell senescence (Fig. 2 D). These findings reveal that SF restructures the LSK epigenome and that a cluster of epigenetic imprinting is retained even after prolonged sleep recovery.

The differentiation capacity of hematopoietic progenitor cells is tightly regulated by stem-intrinsic epigenetic modifications to

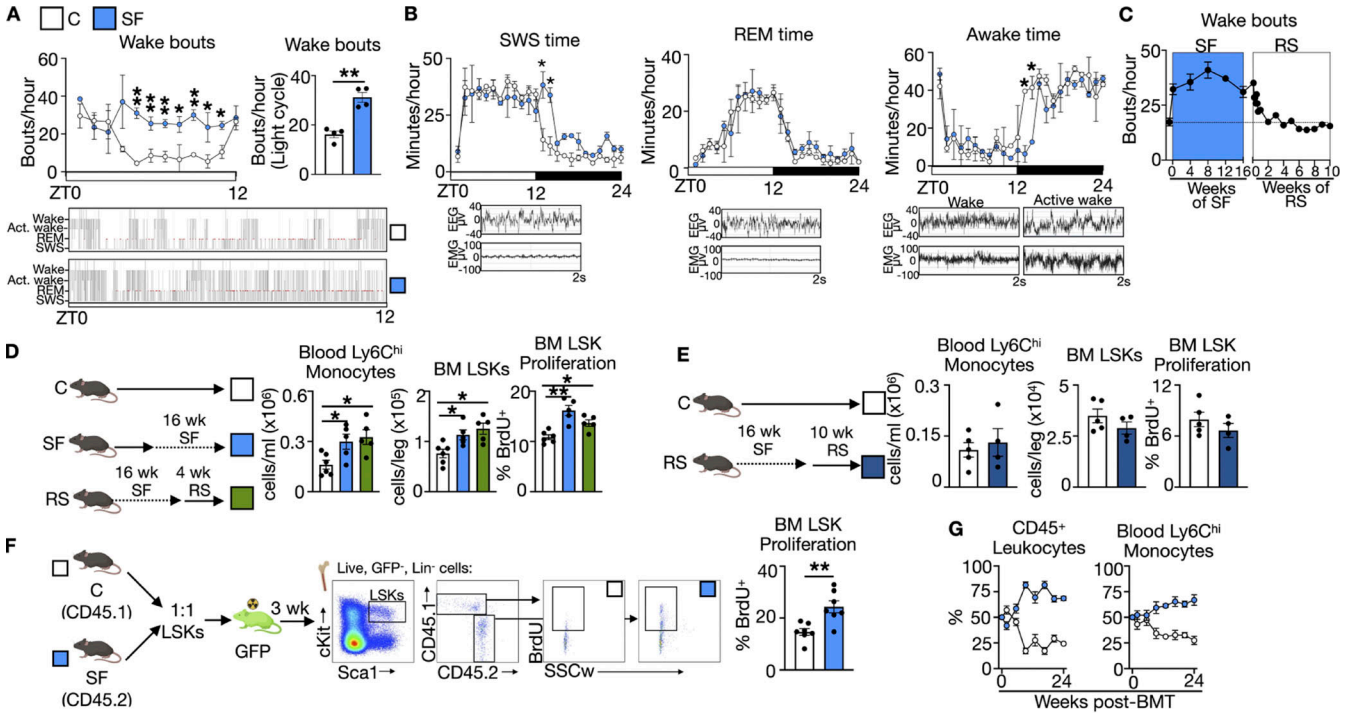

Figure 1. **Sleep exerts a prolonged influence on hematopoiesis. (A)** Quantification of wake bouts (transitions from sleep to wake states), during the resting (light) period along with a representative hypnogram in control (C) and SF mice. *n* = 4 mice per group. **(B)** Quantification of minutes per hour in SWS, REM sleep, and awake time, along with representative EEG and EMG traces, in control and SF animals over 24 h. *n* = 4 mice per group. **(C)** Quantification of resting period wake bouts over 16 wk of SF followed by 10 wk of RS. *n* = 4 mice per group. **(D)** Enumeration of blood Ly6C^{hi} monocytes and BM LSKs, along with LSK BrdU incorporation in control mice, SF mice, and mice exposed to 16 wk of SF followed by 4 wk of RS. *n* = 5–6 mice per group. **(E)** Enumeration of blood Ly6C^{hi} monocytes and BM LSKs, along with LSK proliferation in a distinct cohort of control mice and mice exposed to 16 wk of SF followed by 10 wk of RS. *n* = 4 mice per group. **(F)** BrdU incorporation into LSKs from control (CD45.1) or SF (CD45.2) mice 3 wk after competitive 1:1 LSK transplantation into a UbiGFP mouse sleeping habitually. *n* = 6–7 mice per group. **(G)** Competitive 1:1 transplantation of LSKs from control (CD45.1) or SF (CD45.2) mice into UbiGFP recipient mice and quantification of CD45.1/2 chimerism among blood leukocytes and Ly6C^{hi} monocytes up to 24 wk after transplantation. *n* = 8 mice per group. Mean ± SEM. *, P < 0.05, **, P < 0.01.

lineage commitment genes (Morrison et al., 1996; Rossi et al., 2005; Dorshkind et al., 2020). We found that SF limited accessibility at enhancers important to lymphocyte lineage differentiation (e.g., *Bcl11a*, *Ftl3*, *Sox4*, *Icos*, *Il15*, *Rag1*, *Pax5*, *Ets1*, and *Btk*) but augmented accessibility at enhancers associated with myeloid lineage differentiation (*Csf2rb*, *Irf2bp2*, *Dyrk3*, *Erg*, *Klf9*, and *Klf3*), suggesting SF restricts lymphoid differentiation and drives LSKs toward a myeloid fate (Fig. 2 E). Many changes in myeloid enhancers, but not lymphoid enhancers, were retained after 10 wk of sleep recovery, demonstrating long-term imprinting of sleep on lineage programming. Enhancers associated with cell cycle regulators (*Cdk11b*, *Cdk18*, *Cdkn1b*, and *Cdkn2b*) were also influenced by SF (Fig. 2, E and F). In agreement with our ATAC-seq findings, transcript expression of the cell cycle inhibitors *Cdkn1b* and *Cdkn2b* was reduced in LSKs of SF mice and remained diminished during recovery, while the cyclin *Cdkal1* and the mediators of lineage fate *Klf9* and *Klf3* were increased in SF mice and remained elevated during recovery (Fig. 2 G). These analyses suggest that SF skews the hematopoietic system toward the myeloid lineage, and the capacity for lymphoid differentiation declines due to stem-intrinsic regulation of lineage commitment genes.

The LSK epigenome instructs secondary recall responses and adaptability (Khan et al., 2020; Divangahi et al., 2021; Rodrigues et al., 2021), so we sought to determine whether the preserved epigenetic signature shapes LSKs' response to a subsequent immunological challenge. We allowed mice to either sleep habitually or exposed them to 16 wk of SF and 10 wk of RS before subjecting both groups to cecal ligation and puncture (CLP), a model of sepsis and systemic bacteremia (Fig. 2 H). 24 h after the CLP, despite equivalent blood bacteremia (Fig. 2 I), mice exposed to SF followed by RS developed an exaggerated inflammatory response that included heightened blood monocytes and BM LSKs, accelerated LSK proliferation (Fig. 2 I), and augmented plasma IL-6 and TNFα levels (Fig. 2 J), but unchanged plasma growth factor and corticosterone levels (Fig. S1 M). This heightened inflammatory response associated with a worsened clinical score and reduced survival (Fig. 2 K). To test whether the phenomenon was intrinsic to hematopoietic cells, we transplanted BM cells from control or SF mice into irradiated recipients with no history of sleep disruption (Fig. 2 L). 10 wk after the BM transfer, recipients had equivalent blood monocyte counts regardless of whether they received control or SF BM cells (Fig. 2 M). Recipients were then exposed to CLP and tissues were harvested 24 h later. Mice that received BM cells from SF mice responded more aggressively to CLP with increased blood monocytosis (Fig. 2 N), augmented BM hematopoiesis (Fig. 2 O),

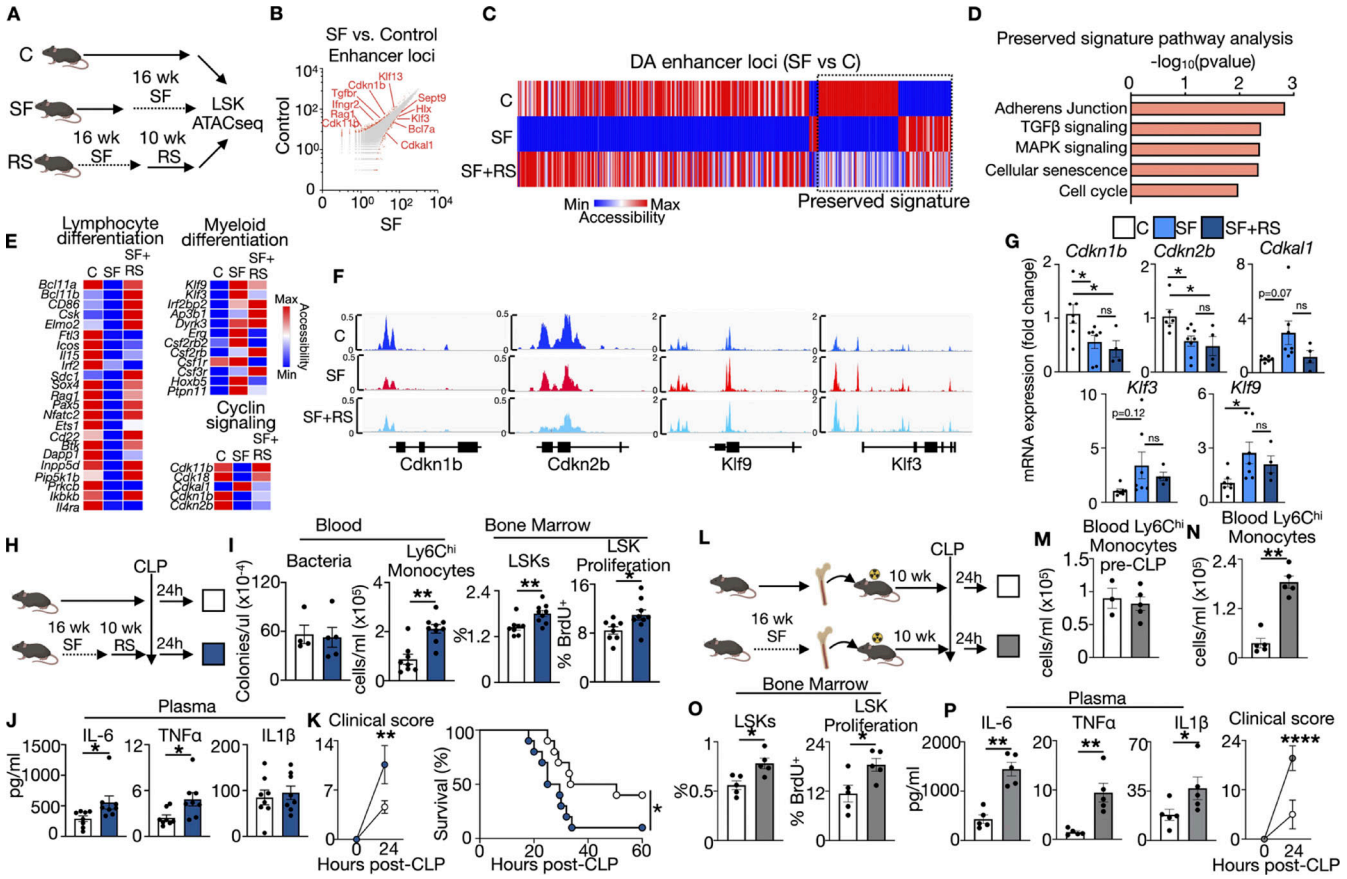

Figure 2. **Sleep programs the LSK epigenome and confers adaptability. (A)** Experimental schematic. C, control. **(B)** Distribution of DA ($Log_2FC > 2$, $P < 0.05$, red circles) enhancer loci in control and SF LSKs. **(C)** Accessibility heatmap of DA enhancer loci between control and SF LSKs and corresponding accessibility in RS group, indicating preserved signature of loci not significantly different ($Log_2FC < 2$, $P < 0.05$) between SF and RS. **(D)** Kyoto Encyclopedia of Genes and Genomes pathway analysis of the retained signature. **(E)** Heatmap of enhancer loci associated with genes important to lymphocyte differentiation, myeloid differentiation, and cyclin signaling. For ATAC-seq analysis, $n = 2$ mice per group, repeated twice, for a total of $n = 4$ per group. **(F and G)** Representative peak map (F) and quantitative PCR analysis (G) of *Cdkn1b*, *Cdkn2b*, *Cdkal1*, *Klf9*, and *Klf3* expression in LSKs of control, SF, and SF+RS mice ($n = 4–7$ mice per group). **(H)** Experimental set up, CLP. **(I)** Blood bacteremia and Ly6C^{hi} monocytes along with BM LSKs and proliferation 24 h after CLP. $n = 4–8$ mice per group. **(J)** Plasma cytokine levels. $n = 8$ mice per group. **(K)** Clinical score ($n = 8$ mice per group) and survival ($n = 10$ mice per group) after CLP. **(L)** Schematic of experimental design. **(M and N)** Blood monocyte numbers immediately prior to (M) and 24 h after (N) the CLP. $n = 3–5$ mice per group. **(O)** BM LSKs and proliferation 24 h after CLP. $n = 5$ mice per group. **(P)** Plasma cytokine levels and clinical score after CLP. $n = 5$ mice per group. Mean ± SEM. *, $P < 0.05$; **, $P < 0.01$; ***, $P < 0.001$; ****, $P < 0.0001$.

and increased plasma cytokine levels, leading to a worsened clinical score (Fig. 2 P), indicating these phenotypes are mediated by leukocyte-intrinsic mechanisms. As an alternate re-challenge model, mice subjected to 16 wk of SF and 10 wk of RS were re-exposed to SF. Mice experiencing a second bout of SF developed monocytosis and elevated LSK proliferation more rapidly relative to mice experiencing SF for the first time (Fig. S1 N). Together, these findings suggest that SF creates memory by priming LSKs, leading to augmented inflammatory responses to subsequent immune challenges.

Given our findings, we hypothesized that modifiers of histone acetylation or epigenetic readers might control these lasting effects. To test this hypothesis, we exposed mice to 4-phenylbutyrate (4PBA), a potent HDAC inhibitor, during weeks 8–16 of SF. HDAC inhibition did not influence body weight but did blunt SF-induced LSK expansion and the expression of proliferation- and lineage-related genes (Fig. S2). After HS or SF, with and without 4PBA treatment, mice underwent RS (while drinking regular water) followed by CLP (Fig. 3 A). After CLP, HDAC inhibition attenuated monocytosis, LSK expansion, LSK proliferation, and plasma cytokines (Fig. 3, B and C). Similarly, inhibition of bromodomain and extraterminal reader proteins (Nicodeme et al., 2010; Fig. 3 D) restricted the secondary inflammatory response including monocytosis (Fig. 3 E), BM hematopoiesis (Fig. 3 F), and plasma cytokine levels (Fig. 3 G). These observations support the idea that SF primes LSKs through epigenetic reprogramming, rendering adaptability to subsequent inflammatory responses.

Sleep maintains hematopoietic clonal diversity

Having shown that SF has sustained effects on the LSK epigenome, lineage commitment, and turnover, we considered possible implications of these perturbations on somatic evolution of the LSK population. The expansion of hematopoietic clones and the homogenization of the hematopoietic system is a common age-associated premalignant condition known as clonal

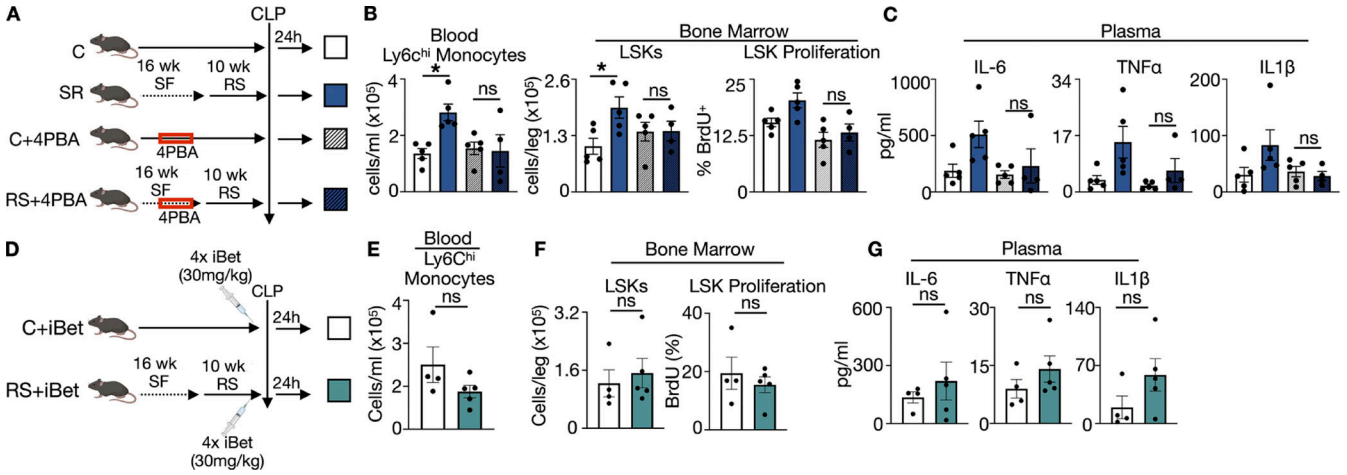

Figure 3. **Sleep-controlled immune adaptability is blunted by epigenetic modifiers. (A)** Experimental schematic of 4PBA delivery. C, control. **(B)** Blood monocyte numbers and BM LSKs and proliferation 24 h after CLP. *n* = 4–5 mice per group. **(C)** Plasma cytokine levels 24 h after CLP. *n* = 4–5 mice per group. **(D)** Experimental schematic of iBet delivery. **(E)** Blood monocytosis 24 h after CLP. *n* = 4–5 mice per group. **(F)** BM LSKs and proliferation 24 h after CLP. *n* = 4–5 mice per group. **(G)** Plasma cytokine levels 24 h after CLP. *n* = 4–5 mice per group. Mean ± SEM. *, P < 0.05.

hematopoiesis (CH; Jaiswal et al., 2014). CH can be driven by accrual of somatic mutations, most commonly in the epigenetic modifiers *Tet2* and *Dmnt3a* (Genovese et al., 2014). CH is associated with accelerated epigenetic aging of HSPCs (Nachun et al., 2021), a twofold increased clinical risk of CVDs (Jaiswal et al., 2017), and all-cause mortality (Jaiswal et al., 2014). Recently, we showed that increased HSPC proliferation caused by SF accelerates the emergence of *Tet2*-mutant CH (Heyde et al., 2021). Specifically, in mixed chimeric animals exposed to SF, *Tet2*-mutant cells expand at a faster rate relative to animals whose sleep was unaltered, resulting in mutants encompassing a greater proportion of blood myeloid cells and BM HSPCs (Heyde et al., 2021). However, the majority of CH cases arise in the absence of detectable driver mutations (Zink et al., 2017; Poon et al., 2021; Mitchell et al., 2022). We predicted that heightened proliferation of HSPCs would not only accelerate the expansion of mutant clones but would also expedite neutral evolution—random fluctuations in mutant frequencies due to stochastic loss and self-renewal of HSPCs (Heyde et al., 2021). Even in the absence of mutant selection, diversity declines over time in stochastically self-renewing stem cell populations due to neutral drift (Snippert et al., 2010), an effect that is accelerated under conditions of increased cell turnover. We set out to investigate experimentally our theoretical prediction that drift would be accelerated in mice subjected to SF (Heyde et al., 2021).

We utilized a multicolor LSK clonal-tracking system (Yu et al., 2016; Shen et al., 2021). Briefly, sorted LSKs were stochastically and permanently tagged ex vivo with up to seven fluorophores and transplanted into lethally irradiated recipient mice (Fig. 4 A). Flow cytometry and a binary gating strategy allowed us to track 127 clusters that incorporated at least one tag and had a unique fluorophore combination (Fig. 4 B). We evaluated tagged LSK clusters and their descendants, which retained the fluorescent tag of the progenitor cell from which they were derived. First, we confirmed that 126 clusters (99%) were detectable among the tagged LSK cells prior to transplantation into recipient mice (Table S1 and Fig. S3 A). 6 wk after transplantation, 110 ± 3 clusters (87%) were detectable among blood leukocytes (Fig. S3 B), with minimal variability between recipient mice (Fig. S3 C). Cluster frequency of blood monocytes and neutrophils correlated remarkably with cluster frequency of BM LSKs (Fig. S3 D), demonstrating that changes in cluster abundance and dynamics in the blood are reflective of changes among BM hematopoietic progenitors.

We subjected the recipient mice to HS or SF and analyzed cluster dynamics in the blood over time. First, we measured the relative change in frequency of clusters with four or more tags, which represent rare and more homogeneous clusters (Table S1). Among blood monocyte and neutrophil clusters, we found that over time, the range of cluster frequencies, the change in mean cluster frequency, and the cluster variance were substantially elevated in SF mice (Fig. 4, C and D), signifying that SF accelerates the expansion of some clusters and the disappearance of others, consistent with expedited neutral drift. We did not observe changes in relative mean cluster frequency, range, or variance among B and T cell populations, presumably owing to the long half-life of these cells (Fig. S4, A and C; Heyde et al., 2021). To directly quantify the evolution of diversity and neutral drift over time, we computed Simpson's diversity index (SDI). We found that in control animals, the SDI of blood monocytes and neutrophils decreased gradually over time (Fig. 4, E and F). In SF mice, however, monocyte and neutrophil SDI decayed more rapidly (Fig. 4, E and F), consistent with the effects of accelerated neutral drift due to increased cell turnover. We did not observe an influence of SF on lymphocyte SDI (Fig. S4, B and D). Together, these data show that SF increases stochastic fluctuations in the frequencies of neutral clusters, thereby reducing hematopoietic cell diversity over time.

Having observed diversity decay through accelerated neutral drift among circulating myeloid cells of SF mice, we turned our attention to progenitors in the BM. Among BM LSKs, 18 wk of SF increased the mean variance of cluster frequencies and

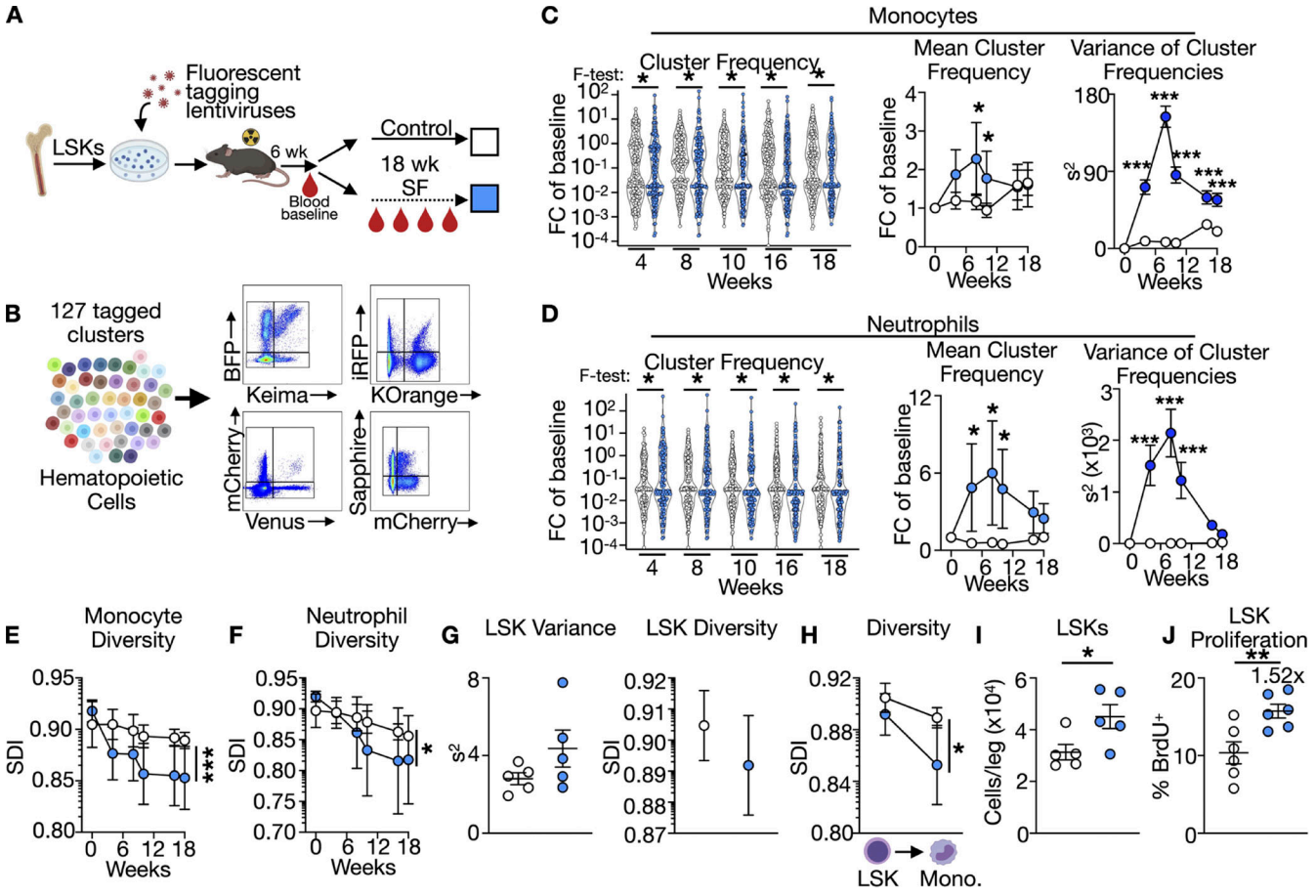

Figure 4. **Sleep maintains hematopoietic diversity and limits neutral drift. (A)** Experimental setup to generate tagged LSKs and transplantation into recipient mice. **(B)** Representative flow cytometry plots of leukocyte clusters in the blood. **(C)** Change in cluster frequency relative to baseline, mean cluster frequency, and variance of cluster frequencies of monocytes with four or more tags. **(D)** Change in cluster frequency relative to baseline, mean cluster frequency, and variance of cluster frequencies of neutrophils with four or more tags. **(E)** SDI among all 127 tagged monocyte clusters. **(F)** SDI among all 127 tagged neutrophil clusters. **(G)** Variance of LSK frequencies (P = 0.16) and SDI (P = 0.27) among 127 tagged LSK clusters after 18 wk of SF. **(H)** SDI of BM LSKs and blood monocytes at sacrifice. **(I)** Enumeration of BM LSKs in recipient mice. **(J)** LSK proliferation after 18 wk of SF. In all panels, *n* = 5 mice per group, except J where *n* = 6 mice per group. Mean ± SEM. *, P < 0.05; **, P < 0.01; ***, P < 0.001.

decreased the SDI (Fig. 4 G), providing direct evidence for accelerated neutral drift and reduced diversity amongst hematopoietic progenitors. To garner insights into the impact of sleep on population diversity as LSKs differentiate into mature cells, we assessed relative changes in the SDI of BM LSKs and circulating cells. We found that in both control and SF mice, diversity was higher in BM LSKs than in differentiated blood cells (Fig. 4 H and Fig. S4 E), reflective of the multipotency and unequal contribution of LSKs to circulating immune cells (Pietras et al., 2015). The reduction in SDI between BM LSKs and blood monocytes was greater in SF animals (Fig. 4 H and Fig. S4 E), suggesting that SF limits diversity during monocyte generation. These findings demonstrate that sleep maintains the diversity and restricts the neutral drift of BM hematopoietic stem and progenitor cells by limiting cell turnover.

Next, we tested whether the rate of SF-induced LSK proliferation inferred from our clonal tracking data was quantitatively consistent with independent experimental observations. We mathematically modeled LSK evolution based on the Moran process of population genetics (see Materials and methods). For this model, we calculated that the LSK SDI decays at a rate proportional to the rate of cellular proliferation divided by the population size. Using the observed LSK population size after 18 wk of SF (Fig. 4 I and Table S2), our model estimated a 1.56 ± 0.26-fold increase in LSK proliferation in SF mice. We confirmed this mathematical prediction experimentally by measuring a 1.52-fold increase in BrdU incorporation in LSKs of SF mice (Fig. 4 J). Using complementary mathematical and experimental methods, our data provide evidence that SF accelerates LSK proliferation and thus neutral drift, rendering the population more homogeneous over time.

Sleep restriction enhances hematopoietic activity and monocytosis in humans

Having established a role for sleep in maintaining the LSK epigenome, immune memory, and clonal diversity in mice, we turned our attention to humans. To test the influence of sleep on hematopoiesis and the epigenome of human hematopoietic progenitor cells, we collected blood samples from humans participating in a randomized crossover study in a free-living

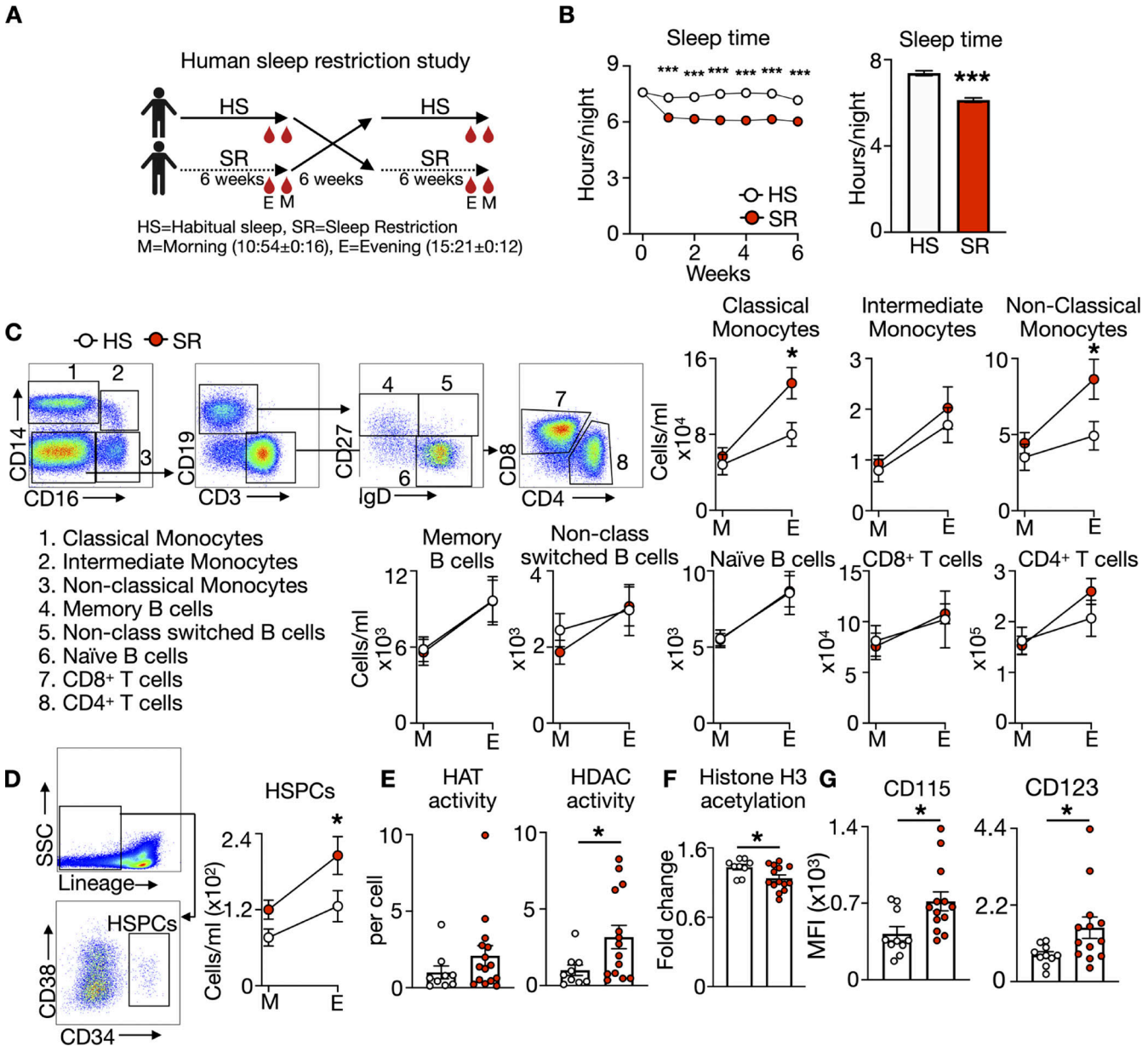

Figure 5. **Human SR promotes monocytosis and shapes the HSPC epigenome. (A)** Schematic of crossover SR study (n = 14). **(B)** TST of subjects during the HS phase and the SR phase measured weekly and averaged over the phase. **(C)** Enumeration of leukocyte populations in the blood during the morning (M) and evening (E) at the completion of each phase. **(D)** Enumeration of lineage⁻CD34⁺ HSPCs. **(E)** HAT and HDAC activity in lineage⁻CD34⁺ HPCs at the evening time point. **(F)** Histone H3 acetylation in lineage⁻CD34⁺ HSPCs at the evening time point. **(G)** Mean fluorescence intensity (MFI) of CD115 and CD123 on HSPCs at the evening time point. Mean ± SEM. *, P < 0.05; ***, P < 0.001.

setting in which chronic mild insufficient sleep was imposed on healthy young volunteers (mean age 35.7 ± 15.1 yr) with adequate HS duration and free of sleep disorders (Fig. 5 A, study flow chart in Fig. S5 A, cohort characteristics in Table S3). The study comprised a 6-wk HS phase where participants slept an average of 7.4 ± 0.1 h per night and a 6-wk SR phase where participants restricted their sleep to 6.1 ± 0.1 h per night (Fig. 5 B). Participants underwent both study phases, in a random order, which were separated by a washout period of 4–6 wk. As participants completed each phase, we collected blood in the morning (mean clock time 10:54 ± 0:16) and evening (mean clock time 15:21 ± 0:12), and analyzed circulating leukocyte populations by flow cytometry. As expected, we detected a circadian pattern characterized by high circulating leukocyte numbers in the evening and low numbers in the morning (Fig. 5 C). However, we found that after completing SR, participants had more circulating CD14⁺CD16⁻ classical monocytes and CD14⁻CD16⁺ nonclassical monocytes in the evening, but not morning (Fig. 5 C). SR did not change intermediate monocytes or B and T cell populations (Fig. 5 C) and changes in blood monocytes did not depend on energy intake or adiposity (Fig. S5 B). Consistent with our murine findings, these data reveal that sleep protects against

blood monocytosis in humans, a phenomenon observable in both species at the start of the resting period (McAlpine et al., 2019).

To build on these observations, we sought to determine whether sleep affects HSPCs in humans. Human lineage⁻CD34+ HSPC numbers fluctuated in the blood according to a circadian rhythm (Fig. 5 D). We found that SR increased HSPC number in the blood in the evening (Fig. 5 D), suggesting that, like in the mouse, SR enhances hematopoietic activity in humans. The impact of SR on HSPCs did not depend on energy intake or adiposity (Fig. S5 C). Next, we investigated whether SR influences the epigenome of human HSPCs. We measured histone acetyltransferase (HAT) and HDAC activity in sorted HSPCs retrieved in the evening and found that SR tended to increase HAT activity and significantly augmented HDAC activity (Fig. 5 E), which reduced histone H3 acetylation (Fig. 5 F) and indicated that sleep shapes the epigenome of human HSPCs. As HSPCs differentiate into myeloid cells, they rely on growth factors CSF1 and IL-3 (Mindur and Swirski, 2019), which signal via CD115 and CD123, respectively. Accordingly, we found enhanced expression of CD115 and CD123 on HSPCs retrieved from participants experiencing SR (Fig. 5 G). These findings reveal that human sleep mediates hematopoiesis, shapes the HSPC epigenome, and promotes myeloid differentiation cues.

Discussion

Sleep profoundly influences the immune system and its functioning (Besedovsky et al., 2019; Irwin, 2019). However, sleep's impact on hematopoiesis and the programming and clonality of HSPCs have remained unclear. Here, we report that murine SF augments sleep–wake transitions, increases hematopoiesis, and alters the epigenome of HSPCs through changes in histone acetylation. While hematopoiesis recedes during sleep recovery, HSPCs retain epigenetic imprinting, priming them for myeloid-biased responses and increased inflammatory activation during subsequent immune challenges. Using a multicolor clonal-tracking system, we find that SF reduces the diversity of the hematopoietic system by accelerating neutral drift and the emergence and disappearance of HSPC clones. In humans, we show that 6 wk of mild SR increases the number of HSPCs and monocytes in the blood, reduces HSPC histone acetylation, and promotes HSPC myeloid response cues. Together, these findings suggest that oscillations in sleep quality and abundance compromise HSPC epigenetic structure, diversity, and subsequent immune function.

Chronic sleep disruption is pervasive in modern lifestyles (Ford et al., 2015). Sleep disruption encompasses many permutations including, but not limited to, fragmentation, restriction, social jet lag, obstructive sleep apnea (OSA), and insomnia, which substantially increase susceptibility to immune-associated diseases (Irwin, 2019). Individuals typically do not experience one continuous form of sleep disruption but oscillate between types of sleep disturbances and between periods of inadequate sleep and healthy sleep. To understand the mechanistic links between sleep on chronic age-associated diseases that develop over decades, fluctuations in sleep patterns must be considered. One mechanism by which even short periods of poor sleep might impact future disease pathology is through epigenetic programming. Insufficient sleep, sleep disorders, and shift work markedly alter a cell's epigenome. For example, OSA modifies the epigenome in the cardiovascular system and circulating leukocytes (Chen et al., 2019), and one sleepless night changes DNA methylation in liver and muscle tissue at the transcription start sites of genes associated with metabolism (Cedernaes et al., 2018). Moreover, sleep disorders, including OSA, insomnia, and sleep-disordered breathing, alter DNA methylation and accelerate the epigenetic age of blood leukocytes (Carroll et al., 2017; Li et al., 2019). Together, these data suggest that sleep modifies the epigenome of diverse cell types throughout the body. However, it has remained unclear whether these sleep-mediated epigenetic modifications have a subsequent consequence on future cell function, inflammation, and disease pathology. Moreover, the influence of sleep on the epigenetic status of HSPCs was unknown. We provide evidence for sustained epigenetic imprinting of HSPCs by sleep disruption. Our data show that SF-induced epigenetic programming is partially maintained during prolonged convalescent sleep and predisposes the hematopoietic system to overt inflammatory responses to subsequent immune challenges. The preserved epigenetic signature is not sufficient for sustained LSK proliferation and differentiation during sleep recovery, likely owing to the vast genomic program and alternate epigenetic modifications, like methylation, involved in controlling cellular proliferation. These data have important implications for inflammatory diseases such as sepsis, CVD, and cancer, and may suggest that early life sleep behavior dictates future disease severity. Our findings support the hypothesis that periods of poor sleep, even if followed by sleep recovery, have sustained consequences on immunological health.

The systemic networks that connect sleep with HSPC epigenetic rewiring and adaptability require further study. Neural circuits together with neuropeptidergic, neuroendocrine, and inflammatory pathways are likely involved. For example, hypothalamic hypocretinergic signaling controls sleep-mediated HSPC proliferation (McAlpine et al., 2019), and our data suggest that SF raises, while sleep recovery normalizes systemic IL-6 levels. IL-6 signaling has broad functionality in health and disease (Libby and Rocha, 2018; Ridker and Rane, 2021), and has been linked to sleep and its disruption (Friedman et al., 2005; Hong et al., 2005; Dimitrov et al., 2006) and histone modifications (Samanta et al., 2008). How IL-6 or other immune signaling factors might fit within the sleep–hematopoiesis–epigenome interaction and mediate adaptability after sleep recovery should be explored in detail.

The HSPC epigenome dictates fate, division, and clonality, and mediates age-associated changes to the hematopoietic system (Morrison et al., 1996; Buisman and de Haan, 2019; Rodrigues et al., 2021). Clonally expanded HSPCs often harbor mutations in epigenetic modifiers, and CH is strongly associated with epigenetic age acceleration (Genovese et al., 2014; Nachun et al., 2021). Therefore, we hypothesized that epigenetic reprogramming and increased proliferation of HSPCs promoted by sleep disruption may influence their clonality and the neutral evolution of the hematopoietic system. Our prior mathematical

framework suggested that the magnitude of HSPC clonal expansion is dependent on their proliferative rate and less on their mutations or conferred fitness advantage (Heyde et al., 2021). For example, increased hematopoiesis induced by SF or high-fat-diet feeding accelerates the emergence and clonal expansion of *Tet2*-mutant HSPCs (Heyde et al., 2021). The theory predicted that a stochastic elevation in hematopoiesis would accelerate neutral drift and the emergence of clones, even in the absence of mutant selection. Here, we used a fluorescent tagging system to test this theory experimentally. We found that increased proliferation of mutant-free HSPCs caused by SF accelerates neutral drift, which leads to faster expansion and disappearance of HSPC clones, thus limiting hematopoietic diversity. Our observations support the notion of reverse causality–increased HSPC proliferation accelerates the expansion of mutant and neutral clones. These data add to our understanding of the relationship between CH and inflammatory disorders such as CVD whose risk factors, including sleep disruption, augment hematopoiesis and expedite the emergence of mutant and nonmutant HSPC clones, increasing disease susceptibility.

Humans experiencing SF (Vallat et al., 2020) and OSA (Geovanini et al., 2018) develop blood monocytosis and neutrophilia. However, the influence of sleep on hematopoiesis, HSPC function, and circadian dynamics in humans had not been explored. We found that 6 wk of chronic mild SR increased the number of blood monocytes and HSPCs in human subjects, but did not influence lymphocyte populations. Whether the elevation in blood HSPCs is due to increased hematopoietic activation through augmented HSPC cycling in the BM and/or increased HSPC release from the BM will require further study. Importantly, these findings were observed in the evening, mirroring our murine data (McAlpine et al., 2019) and suggesting that the time of blood collection is a critical variable when assessing changes in blood leukocyte number. Additionally, our findings reveal that SR alters the intrinsic epigenome of human HSPCs by reducing histone acetylation through increased HDAC activity. Together, our murine and human data propose that different forms of sleep interruption in species with dissimilar sleep architecture perpetuate similar outcomes on hematopoiesis and monocytosis, underscoring the preserved nature of this phenomenon.

Understanding the prolonged influence of sleep on immune function and disease susceptibility is important, particularly given the nearly pandemic prevalence of insufficient sleep (Watson et al., 2015). Our study provides evidence, in mice and humans, that sleep exerts a lasting influence on the immunity and functioning of HSPCs via epigenetic modification, and that SF genetically ages the hematopoietic system by accelerating neutral drift, which collapses clonal diversity and homogenizes the myeloid pool.

Materials and methods

Animal studies

Wild-type C57BL/6J, B6.SJL-Ptprca Pepcb/BoyJ (CD45.1), and C57BL/6-Tg(UBC-GFP)30Scha/J (ubiGFP) mice were purchased from The Jackson Laboratory. Age- and sex-matched mice were used. Where appropriate, mice were randomly assigned to interventions. All mice were group-housed with free access to food and water. All animal protocols were approved by the Animal Review Committee at the Massachusetts General Hospital (protocol nos. 2011N000035 and 2015N000044) or the Icahn School of Medicine at Mount Sinai (protocol nos. PROTO202100023 and PROTO202000262) and were in compliance with relevant ethical regulations.

In vivo interventions

SF and RS

For SF, studies were performed as previously described (McAlpine et al., 2019). Briefly, mice were placed in an SF chamber (Lafayette Instrument) and the sweep bar moved along the bottom of the cage every 2 min during the light cycle (ZT0–12). The sweep bar automatically shut off and was stationary during the dark cycle (ZT12–24). Control mice whose sleep was unaltered were placed in SF chambers with stationary sweep bars. For recovery experiments, the sweep bar was shut off and animals were transferred to a conventional mouse cage.

Telemetry EEG and EMG monitoring

First, animals were implanted with EEG/EMG transmitters (HDx-02; Data Science International). Briefly, the head of the animal was secured in a stereotactic frame and a 2–3 cm incision was made along the dorsal midline posterior margin of the eyes to midway between the scapulae. A subcutaneous pocket was formed and the implant was inserted with the biopotential leads oriented cranially. The EMG electrodes were inserted into the cervical trapezius muscle in the dorsal region of the neck and the ends were sutured so they remain in place. To place the EEG electrodes, a microdrill was used to perforate the skull above the cortex. The ends of the leads were placed in the hole such that they make contact with the dura of the cortex. The leads were secured in place using dental acrylic. The skin incision was sutured and mice received postsurgical analgesia and were supplemented with warmth for 1 h. Mice were allowed to recover for 1 wk before monitoring began. Mice were placed in SF or control chambers and EEG/EMG data was recorded using the Data Science International (DSI) telemetry system and hardware. Ponemah software (DSI) was used to acquire the data, and Neuroscore 3 (DSI) was used to perform sleep analysis using standard settings.

BM transplantation

For competitive transplantation assays, mice were lethally irradiated (950 cGy) and reconstituted with 50,000 LSKs from each donor along with 2,000,000 BM feeder cells (of the same genotype as the recipient mouse) injected intravenously 18 h after irradiation.

CLP

The CLP procedure was carried out as previously described (Weber et al., 2015). Briefly, the peritoneal cavity was opened during isoflurane anesthesia and the cecum was exteriorized and ligated at the second arterial vessel or third arterial vessel (for survival studies) distal to the end of the cecum. The ligated portion of the cecum was then perforated using a 17-G needle, and a small drop of cecal content was extruded through the

puncture. The cecum was relocated into the peritoneal cavity and the peritoneum was closed. Animals were given 1 ml of saline and removed from isoflurane.

Reagent administration

4PBA was dissolved in water at a concentration of 5.75 g/liter, which results in a delivery of ∼1.5 g/kg/d when given as drinking water. 4PBA-containing drinking water was given to mice at week 8 of SF, removed at week 16, and changed weekly. iBet was dissolved in 20%β-cyclodextrin and 11% DMSO and intravenously injected into animals at a concentration of 30 mg/kg four times over 2 d prior to CLP.

Cells

Collection

Peripheral blood was collected at ZT3 by retro-orbital bleeding, and red blood cells were lysed in RBC lysis buffer (Biolegend). BM cells were collected at ZT3 by flushing bones with PBS, after which a single-cell suspension was created by passing cells through a 26-gauge needle and red blood cells were lysed with RBC lysis buffer. Total viable cell numbers were counted using trypan blue (Cellgro; Mediatech) or counting beads (Thermo Fisher Scientific).

Flow cytometry

Single-cell suspensions were stained in PBS supplemented with 2% FBS and 0.5% BSA. The following monoclonal antibodies were used for flow cytometry analyses: anti-CD45 (clone30-F11, 103147; BioLegend), anti-CD45.1 (clone A20, 110708; BioLegend), anti-CD45.2 (clone 104, 109802; BioLegend), anti-CD3 (clone 17A2, 100206; BioLegend), anti-CD90.2 (clone 53-2.1, 105308; BioLegend), anti-CD19 (clone 6D5, 115508; BioLegend), anti-B220 (clone RA3-6B2, 553089; BD Biosciences), anti-NK1.1 (clone PK136; BioLegend), anti-Ly-6G (clone 1A8, 127614; BioLegend), anti-Ly-6C (AL-21, 128006; BioLegend), anti-CD11b (clone M1/70, 101226; BioLegend), anti-CD115 (clone AFS98, 135517; BioLegend), anti-Ter119 (clone TER-119, 116208; BioLegend), anti-CD34 (clone RAM34, 11-0341-85; eBioscience), anti-CD49b (clone DX5, 1089008; BioLegend), anti-CD11c (clone N418, 117310; BioLegend), anti-IL-7Rα (clone SB/199, 121112; BioLegend), anti-CD16/32 (clone 93, 101324; BioLegend), anti-cKit (clone 2B8, 105814; BioLegend), anti- Sca1 (clone D7, 108126; BioLegend), anti-CD8 (clone 53-6.7, 553035; BD Bioscience), anti-CD4 (clone GK1.5, 100428; BioLegend), and anti-BrdU (clone BU20A, 17-5071-42; eBioscience). All antibodies were used in a 1:700 dilution. Viable cells were identified as unstained with 7AAD (BioLegend). Cells were identified as Ly-6Chigh monocytes ($CD45^+CD11b^+CD115^+Ly^-6Chigh$), neutrophils ($CD45^+CD11b^+Ly^-6G^+$), LSK cells ($CD45^+Lin^-Kit^+Sca1^+$), B cells ($CD45^+B220^+CD19^+CD11b^-$), and T cells ($CD45^+CD3^+CD90^+CD8^+CD11b^-$). Lineage was B220, CD19, CD49b, Ter119, CD90.2, CD11b, CD11c, Ly-6G, and IL-7Rα. Viable cells were identified as unstained with 7AAD (Biolegend). Data were acquired on a LSRII and a FACS Aria II (BD Biosciences) and analyzed with FlowJo (Tree Star).

BrdU incorporation

To assess cell proliferation, 1 mg BrdU was injected intraperitoneally 2 h before euthanasia. A BrdU flow kit (BD Biosciences) was used to stain BrdU+ cells.

Cell sorting

BM cell suspensions were stained to identify the indicated cell populations, and cells were sorted on a FACS Aria II cell sorter (BD Biosciences) directly into collection medium.

Molecular analysis

Quantitative PCR

Total RNA was isolated using the RNeasy Mini Kit (Qiagen) or the NucleoSpin RNA XS kit (Takara Bio) according to the manufacturer's instructions. RNase-free DNase Set (Qiagen) was used for DNase digestion during RNA purification. RNA quantity and quality were assessed by Nanodrop for RNA isolated from tissues and with the Aglient RNA 6000 Pico kit (Aglient Technologies) on the Aglient 2100 Bioanalyzer for RNA of FACS-purified cells. cDNA was generated from 1 µg of total RNA per sample using the High-Capacity cDNA Reverse Transcription Kit (Applied Biosystems). Quantitative real-time TaqMan PCR was performed using the following TaqMan primers (Applied Biosystems): Mm00438168, Mm00483241, Mm00492956, Mm00495172, and Mm00507441.

Enzyme-linked immunosorbent assay

IL-6, TNFα, IL-1β, M-CSF, and G-CSF levels were measured using an ELISA (Boster Biologics) according to the manufacturer's instructions. On sorted cells, HAT and HDAC activity were measured using commercially available kits, HAT kit (cat#-EP1001; Sigma-Aldrich) and HDAC Kit (cat#CS1010; Sigma-Aldrich), respectively, according to the manufacturer's instructions. Corticosterone was measured using an ELISA (Abcam) and according to the manufacturer's instructions.

ATAC-seq

ATAC-seq was conducted in technical and biological duplicates. Briefly, 20,000 sorted LSK cells were initially resuspended in lysis buffer and centrifuged. The nuclei pellets were then subjected to transposition reaction using the Nextera Tn5 transposase enzyme (Illumina). Tagmented DNA was purified with the MinElute PCR Purification kit and eluted in 10 µl of elution buffer (Qiagen). Barcoded libraries were prepared and PCR-amplified. Double-sided bead purification was performed using AMPure XP beads to remove primer dimers and large >1,000-bp fragments. Libraries were sequenced as 50-bp paired-end reads on an Illumina HiSeq 2500.

Sequencing reads were first mapped to the mm10 reference genome using BWA-MEM66 with default parameters, followed by calling peaks using HOTSPOT2. We identified 41,000 peaks, which showed high consistency between biological duplicates. Peaks with differential accessibility between conditions were identified using edgeR68, with cutoffs of at least a Log_2Fold change>1.2 difference in normalized read density and $P < 0.05$.

Pathway analysis

Kyoto Encyclopedia of Genes and Genomes pathway analysis was done using Enrichr (https://maayanlab.cloud/Enrichr/) with default parameters.

Clinical scoring

Clinical scoring was performed as previously described (Weber et al., 2015). The clinical score of each animal was assessed as

follows (points). [a] appearance: normal (0), lack of grooming (1), piloerection (2), hunched up (3), above and eyes half closed (4); [b] behavior—unprovoked: normal (0), minor changes (1), less mobile and isolated (2), restless or very still (3); behavior—provoked: responsive and alert (0), unresponsive and not alert (3); [c] clinical signs: normal respiratory rate (0), slight changes (1), decreased rate with abdominal breathing (2), marked abdominal breathing and cyanosis (3); [d] hydration status: normal (0), dehydrated (5). The higher the score, the worse the clinical situation of the animal.

Survival analysis

CLP were performed as described above. Animals were then monitored until they reached endpoint.

Bacterial cultures

Whole blood was diluted in PBS, plated on trypticase soy agar with 5% horse blood, and incubated at 37°C. The number of bacterial colonies was assessed 12–16 h later.

Generation of fluorescent-tagged mice and tracking of clusters

Donor WT mice were sacrificed and 1,000,000 BM LSKs were sorted and pooled. LSKs were cultured in serum-free StemSpan medium (StemCell Technologies) containing penicillin, streptomycin, glutamine, and a combination of cytokines (20 ng/ml IL-3, 100 ng/ml SCF, 100 ng/ml Flt-3L, 50 ng/ml thrombopoietin, all from Peprotech) at a concentration of 106 cells/ml. After 1 h of prestimulation, cells were transduced with a mix of highly concentrated lentiviral vectors encoding for different fluorescent proteins (BFP, Sapphire, Venus, KO, mCherry, iRFP, and Keima) at a dose of 20 transducing units/cell. After tagging, a small aliquot of cells was analyzed by flow cytometry prior to their transplantation (BM baseline). Recipient mice were lethally irradiated (9.5 Gy), and each was i.v. injected with 100,000 tagged LSKs along with 2,000,000 Sca1$^-$ unlabeled feeder cells. Mice were allowed to recover and sleep habitually for 6 wk. After recovery, mice were bled and circulating leukocytes were analyzed (blood baseline). Mice were then randomly assigned to SF or HS. Animals were bled periodically and sacrificed after 18 wk of SF.

Mathematical calculations of variance

Cells that fluoresced above background were considered positive for an incorporated fluorescent tag. Distinguishing dichotomous populations (positive or negative for a fluorophore) allowed the identification of 127 uniquely tagged clusters plus one cluster that did not incorporate any fluorophores and was excluded from analysis. Fold change in relative frequencies was calculated by dividing cluster frequency by the baseline frequency. Variance (s^2) of cluster frequency was calculated using the following equation:

$$s^2 = \frac{\sum_{i=1}^{n}(x_i - \bar{x})^2}{n-1},$$

where x is the mean frequency and n is the number of clusters.

Mathematical calculations of Simpson's diversity and cell division rate estimation

For a single mouse, SDI at time t is defined by:

$$D_t = 1 - \sum_{i=1}^{127}(X_{i,t})^2,$$

where $i = 1, .., 127$ denote the tagged clusters and $X_{i,t}$ is the frequency of cluster i at time t. To predict the evolution of Simpson's diversity, we model that LSK's divide and die according to the Moran process (Ewens, 2004), which is parameterized by the number of cells N and the per cell division rate a. From the Kolmogorov equations (Durrett, 2012), the expected Simpson's diversity follows the differential equation

$$\frac{d}{dt}\mathbb{E}D_t = -\frac{2a}{N}\mathbb{E}D_t,$$

which has the solution

$$\mathbb{E}D_t = D_0 e^{-\frac{2a}{N}t}. \quad (1)$$

It follows that

$$\frac{N_S \log\left(\frac{1}{\#S}\sum_{m\epsilon S}\frac{D_{t,m}}{D_{0,m}}\right)}{N_C \log\left(\frac{1}{\#C}\sum_{m\epsilon C}\frac{D_{t,m}}{D_{0,m}}\right)} \quad (2)$$

is a consistent estimator for a_S/a_C, where S is the set of mice in the SF group, C is the set of mice in the control group, $D_{t,m}$ is Simpson's diversity at time t for mouse m, and a_S, a_C, N_S, N_C are the division rates and LSK numbers for the SF and control mice. While control vs. SF mice are expected to have similar LSK numbers at the beginning of the experiment, we measure that LSK numbers are 1.4-fold higher in SF vs. control mice at 18 wk. Averaging over the two time points, we take $N_S/N_C = 1.2 \pm 0.2$. Plugging this into Eq. 2 along with the LSK diversity measurements, an estimate of $a_S/a_C = 1.56 \pm 0.26$ is obtained. That is, LSKs divide at a rate (1.56 ± 0.26)-fold faster in SF vs. control mice, which is consistent with the BrdU estimate of 1.52.

There are caveats to our division rate estimation. For one, the model of LSK evolution is simplistic. A more detailed model could, for example, consider that division rates and LSK numbers may vary over time and between mice in a group. Moreover, there would ideally be more data points to enable improved estimate precision. Nevertheless, the purpose of the modeling is conceptual. We demonstrate that accelerated genetic drift due to increased division rates can explain SF's impact on LSK diversity.

Human study

Study design

The human subjects component of this study employed a randomized crossover design to assess the impact of a common model of chronic insufficient sleep on hematopoiesis in 14 participants. This outpatient trial included two sleep conditions: maintenance of habitual adequate sleep (HS) and prolonged mild SR. Each condition was 6 wk in duration. The order of conditions was randomized across participants, and study phases were separated by a 4–6-wk washout. In the fifth and sixth weeks of each study condition, blood samples were collected in the late afternoon/early evening (hereafter referred to as early evening) and the morning, respectively, for assessment of hematopoietic outcomes. This investigation was a component of an ongoing clinical trial designed to test the impact of prolonged insufficient sleep on energy

balance. The trial was prospectively registered on ClinicalTrials.gov (NCT02960776). All procedures were conducted in accordance with the Declaration of Helsinki and approved by the Columbia University Institutional Review Board (protocol number AAAQ7746); all participants provided informed consent prior to participation.

Subjects

Metabolically healthy men and women, aged 20–75 yr, and with an HS duration of ≥7 h/night, were recruited through advertisements placed online and throughout the New York City area. Individuals meeting initial eligibility criteria based on a phone interview were invited to the laboratory for an in-person screening visit. During this visit, height and weight were measured in duplicate using calibrated research-grade stadiometer and scale (Tanita WB-3000), respectively. Body mass index (BMI) was calculated as weight (kg) divided by height (m) squared. Individuals then completed questionnaires validated for assessment of sleep and circadian rhythms as well as a detailed health history questionnaire. Men and women were deemed potentially eligible if they had overweight or class I obesity (BMI 25.0–34.9 kg/m^2) or were at risk for obesity (BMI 20.0–24.9 kg/m^2 with ≥1 parent with BMI >27 kg/m^2), had good HS quality (score ≤5 on the Pittsburgh Sleep Quality Index [Buysse et al., 1989]), were at low risk for sleep apnea (<2 positive categories on Berlin Questionnaire [Netzer et al., 1999]), and did not report excessive daytime sleepiness (scores <10 on the Epworth Sleepiness Scale [Johns, 1991]). Those with extreme morning or evening chronotypes (scores ≤30, ≥70 on the Morningness-Eveningness Questionnaire [Horne and Ostberg, 1976]), participating in shift work or daytime napping, or had recent travel across time zones (≤3 wk) were not eligible to participate. Exclusion criteria also included current smoking, dieting, recent weight change >2.5 kg, excessive caffeine intake (>300 mg/d), use of hormonal contraceptives, pregnant or ≤1 y postpartum, as well as presence of cardiovascular, metabolic, neurological, or psychiatric diseases or disorders (including eating and substance abuse disorders). Individuals meeting all eligibility criteria were invited to complete an intensive outpatient sleep screening to ensure habitual adequate sleep duration. Sleep was assessed continuously over 2 consecutive weeks using the Actigraph GT3X + (Actigraph Corporation) and nightly sleep diaries. The Actigraph GT3X+ is a triaxial accelerometer worn on the nondominant wrist and validated against polysomnography (Full et al., 2018), the gold standard objective measurement of sleep. Inclusion in the study required a 14-night average total sleep time (TST) of 7–9 h/night with ≥7 h of sleep on ≥ 10 of the nights and no more than 3 nights with <6 h of sleep. To date, 42 participants met these criteria and have been randomly assigned an order of study conditions. Of the full sample, 16 participants (nine women) were accrued for this ancillary study, which began after initiation of the main study; however, two individuals dropped out of the study. Thus, the analytic sample was 14 (n = 7 women).

Intervention

Participants were studied in a free-living setting over 2 phases of 6 wk each, differing only in sleep duration conditions: HS and SR. In both conditions, habitual patterns of sleep, determined from screening, were used to create fixed personalized sleep schedules in both conditions. In the HS condition, participants were to maintain their average bed and waketimes from screening to achieve their habitual adequate sleep duration of ≥7 h/night. In contrast, during SR, participants were instructed to delay their bedtimes (from screening averages), while maintaining habitual wake times, to achieve a reduction in TST of ∼90 min/night. To promote fidelity to the protocol, bed and wake times were adjusted slightly to the participants' preferences. In addition, sleep was monitored continuously using wrist-actigraphy and nightly sleep diaries, and verified weekly by trained study staff throughout the 6-wk study phases to assess compliance. Study phases were separated by a 4–6-wk washout period; sleep was reassessed over the final 2 wk of this washout period to confirm that participants were achieving average TST ≥7 h/night before beginning the next study phase.

Procedures

During each study phase, participants came to the laboratory for a baseline visit (week 0), during which time they completed a number of procedures and received their sleep assignment. Participants returned on a weekly basis for review of wrist-actigraphy data and sleep logs, and for additional assessments. Many of these procedures are beyond the scope of this study. At baseline (week 0) and endpoint visits (week 6), participants underwent MRI scans, and peripheral blood was drawn from a vein within the antecubital fossa into an EDTA tube by a trained phlebotomist while participants were in the fasted state. Blood draws at baseline and endpoint visits (week 6) were scheduled for mornings between 09:00 and 11:00. At a separate visit, 5 wk into each condition, whole blood was collected in the evening (15:00–17:00). The amount of blood collected and time of draw was recorded at all visits and the vast majority of draws (86%) occurred within 1 h of the planned ranges of draw times.

Blood samples were processed shortly after collection for extraction and preservation of the viability of blood cells. Whole blood was transferred to a 50 ml conical tube (Corning) and PBS diluted to 1× (Thermo Fisher Scientific) was added to the blood to a final volume of 35 ml. The solution was then carefully underlaid with 15 ml of Ficoll-Paque PLUS (GE Healthcare) and spun for 30 min at 23°C and 1,800 rpm with the centrifuge brake off (Eppendorf 5810R; Eppendorf). The resulting white blood cell layer was aspirated and transferred to a new conical tube; PBS was added to a final volume of 50 ml and then spun for 10 min at 4°C (1800 rpm, brake on). After spinning, the white blood cell pellet was resuspended in freezing media (20% FBS RPMI 1640 [Thermo Fisher Scientific] with 10% DMSO [Sigma Life Sciences]) and transferred into separate 1.5 ml cryovials. The cryovials were frozen at a controlled rate of −1°C/min (Mr. Frosty; Thermo Fisher Scientific) to maintain viability of cells and were then transferred to liquid nitrogen for storage until flow cytometry analysis. Neutrophils are not included in the leukocytes isolated by Ficoll-Plaque PLUS gradient as they are pelleted and discarded.

Human flow cytometry

For flow cytometry of human leukocytes, cells were quickly warmed in a 37°C water bath. 1 ml of prewarmed RPMI1640 media containing 10% FBS was added to the cells. Cells were

transferred to a 15-ml tube containing 10 ml of 10% FBS RPMI1640 media. Cells were spun at 200 *g* for 10 min and washed in PBS before staining with antibodies. Cells were stained in PBS supplemented with 2% FBS, 0.5% BSA, and 0.5% EDTA. The following monoclonal antibodies (clone) were used at a dilution of 1/700 unless otherwise indicated: anti-CD2 (RPA-2.10), anti-CD3 (HIT3a), anti-CD4 (RPA-T4), anti-CD8 (RPA-T8), anti-CD10 (HI10a), anti-CD11b (ICRF44), anti-CD14 (HCD14), anti-CD16 (3G8), anti-CD19 (H1B19), anti-CD20 (3H7), anti-CD56 (HCD56), anti-CD235 (HI264), anti-CD90 (2E10), anti-CD115 (9-4D2-1E4), anti-CD123 (6H6), anti-CD34 (8G12), anti-IgD (IA6-2), anti-CD27 (M-T271), anti-CD8 (RPA-T8), anti-IgM (MHM88), and anti-CD4 (RPA-T4). Samples were probed with 7AAD to identify live cells. Data were acquired on a LSRII (BD Bioscience) and analyzed with FlowJo (TreeStar).

Human flow cytometry gating strategy

Live, singlet cells were identified as (1) classical monocytes: $CD14^+CD16^-$; (2) intermediate monocytes: $CD14^+CD16^-$; (3) non-classical monocytes: $CD14^-CD16^+$, (4) memory B cells: $CD14^-CD16^-CD19^+$CD27+IgD-; (5) nonclass switched B cells: $CD14^-CD16^-CD19^+$CD27+IgD+; (6) naive B cells: $CD14^-CD16^-CD19^+$CD27-IgD+; (7) $CD8^+$ T cells: $CD14^-CD16^-CD19^-CD3^+CD4^-CD8^+$; (8) $CD4^+$ T cells: $CD14^-CD16^-CD19^-CD3^+CD4^+CD8^-$; and (9) HSPCs: lineage-$CD34^+$. Lineage: CD2, CD3, CD4, CD7, CD8, CD10, CD11b, CD14, CD19, CD20, CD56, and CD235. Viable cells were identified as unstained with 7AAD (Biolegend). Data were acquired on a LSRII (BD Biosciences) and analyzed with FlowJo (Tree Star).

Human cell sorting

Cells suspensions were stained as above and HSPCs were sorted on a FACS Aria II cell sorter (BD Biosciences) directly into collection medium.

Enzymatic activity and histone acetylation

On sorted HSPCs, HAT and HDAC activity along with H3 histone acetylation were measured using commercially available kits according to the manufacturer's instructions: HAT kit (cat#-EP1001; Sigma-Aldrich), HDAC Kit (cat#CS1010; Sigma-Aldrich), and H3 acetylation kit (cat#ab115102; Abcam).

Human energy intake

In the human subjects study, which is ongoing, we collect data on food intake using 3-d food records. Participants are asked to record all foods they consume, in real-time, on three nonconsecutive days (2 weekdays, 1 weekend). Participants are asked to provide detailed information on food brands, ingredients, and amounts and are provided with information on the use of common portion estimation tools. Food records are collected at week 0 (baseline), week 3, and week 6 (endpoint) of each phase. Nutrient analyses are completed in Nutrition Data System for Research (UMinn), and daily averages are calculated from the 3-d records.

Human adiposity

Total volume of adipose tissue and its distribution was measured at baseline and endpoint with MRI using procedures previously described (Shen et al., 2004).

Statistics

Results are shown as mean ± SEM. Statistical analysis was performed using GraphPad Prism 7 (Graphpad Software). Statistical tests included unpaired, two-tailed nonparametric Mann–Whitney *U* tests (when Gaussian distribution was not assumed). For multiple comparisons of more than two groups, a nonparametric multiple-comparisons test comparing the mean rank of each group (when Gaussian distribution was not assumed) was used, along with one- or two-way ANOVAs followed by Tukey's test. For analysis of human data, two-way ANOVAs were performed when comparing multiple groups and time-points, or two-tailed nonparametric Mann–Whitney *U* tests when comparing two groups. Correlation was computed using linear regression. P values of 0.05 or less were considered to denote significance. Each mouse experiment was repeated independently at least two or more times with similar results.

Description of supplementary information

Supplementary tables and figures accompany this manuscript. They describe the influence of SF and RS on inflammation, LSK fitness, epigenetic rewiring, and adaptability; an analysis of mice treated with HDAC inhibitors; numerous quality control metrics of the clonal tracking system; the clonal frequency and diversity metrics of lymphocytes; and a description of the human trial and its participants along with an assessment of human leukocytosis with energy intake and adiposity.

Online supplemental material

Fig. S1 shows the influence of SF and RS on inflammation, LSK fitness, epigenetic rewiring, and adaptability. Fig. S2 is the analysis of mice treated with 4PBA. Fig. S3 shows cluster size and distribution and correlation of cluster frequencies in the BM and blood. Fig. S4 shows the influence of sleep on lymphocyte diversity. Fig. S5 shows the human study. Table S1 provides LSK cluster frequency. Table S2 lists the number of LSKs in recipient control and SF mice. Table S3 provides human subject characteristics at baseline.

Data and materials availability

All data and methods are available and described within. Materials are available upon request.

Acknowledgments

We thank the Harvard Stem Cell Institute-Center for Regenerative Medicine Flow Cytometry Core Facility at the Massachusetts General Hospital (MGH) and the Flow Cytometry CoRE at the Icahn School of Medicine at Mount Sinai for assistance in cell sorting; and the MGH NexGen sequencing and Bioinformatics facility for ATAC-seq experiments and analysis.

This work was funded by the National Institutes of Health (NIH) K99/R00 HL151750, R01 HL158534, and the Cure Alzheimer's Fund (to C.S. McAlpine); an Erwin Schrödinger Postdoctoral Fellowship J4645 by the Austrian Science Fund (to M.G. Kiss); NIH T32 HL007343 and Russel Berrie Foundation Fellowship Award (to F.M. Zuraikat); NIH P01 HL142494 and NIH R35 HL139598 (to M. Nahrendorf); NIH Ruth L. Kirschstein

National Research Service Award Individual Predoctoral Fellowship F31HL147364 (to J.E. Mindur); NIH R35 HL155670, R01 HL128226, and R01 HL142648 (to M.-P. St-Onge); NIH National Center for Advancing Translational Sciences UL1TR001873; and Cure Alzheimer's Fund, NIH R35 HL135752, P01 HL131478, P01 HL142494, and the Patricia and Scott Eston MGH Research Scholar (to F.K. Swirski).

Author contributions: Conceptualization: C.S. McAlpine, M.G. Kiss, F.M. Zuraikat, D. Cheek, R.I. Sadreyev, M. Nahrendorf, K.L. Jeffrey, D.T. Scadden, K. Naxerova, M.-P. St-Onge, F.K. Swirski. Data acquisition: C.S. McAlpine, M.G. Kiss, F.M. Zuraikat, D. Cheek, G. Schiroli, H. Amatullah, P. Huynh, M.Z. Bhatti, L.P. Wong, A.G. Yates, W.C. Poller, J.E. Mindur, C.T. Chan, H. Janssen, J. Downey, S. Singh. Data analysis: C.S. McAlpine, M.G. Kiss, F.M. Zuraikat, D. Cheek, G. Schiroli, H. Amatullah, K. Naxerova, M.-P. St-Onge, F.K. Swirski. Methodology: C.S. McAlpine, M.G. Kiss, F.M. Zuraikat, D. Cheek, G. Schiroli, H. Amatullah, R.I. Sadreyev, M. Nahrendorf, K.L. Jeffrey, D.T. Scadden, K. Naxerova, M.-P. St-Onge, F.K. Swirski. Supervision: R.I. Sadreyev, M. Nahrendorf, K.L. Jeffrey, D.T. Scadden, K. Naxerova, M.-P. St-Onge, F.K. Swirski. Writing: C.S. McAlpine, M.G. Kiss, F.M. Zuraikat, D. Cheek, K. Naxerova, M.-P. St-Onge, F.K. Swirski.

Disclosures: M. Nahrendorf reported receiving funds or material research support from Lilly, Alnylam, Biotronik, CSL Behring, GlycoMimetics, GSK, Medtronic, Novartis, and Pfizer, as well as consulting fees from Biogen, Gimv, IFM Therapeutics, Molecular Imaging, Sigilon, NovoNordisk, Verseau Therapeutics, and Bitterroot. No other disclosures were reported.

Submitted: 13 January 2022
Revised: 21 June 2022
Accepted: 22 August 2022

References

Besedovsky, L., T. Lange, and M. Haack. 2019. The sleep-immune crosstalk in health and disease. *Physiol. Rev.* 99:1325–1380. https://doi.org/10.1152/physrev.00010.2018

Buisman, S.C., and G. de Haan. 2019. Epigenetic changes as a target in aging haematopoietic stem cells and age-related malignancies. *Cells*. 8:868. https://doi.org/10.3390/cells8080868

Buysse, D.J., C.F. Reynolds 3rd, T.H. Monk, S.R. Berman, and D.J. Kupfer. 1989. The Pittsburgh sleep quality index: A new instrument for psychiatric practice and research. *Psychiatr. Res.* 28:193–213. https://doi.org/10.1016/0165-1781(89)90047-4

Carroll, J.E., M.R. Irwin, M. Levine, T.E. Seeman, D. Absher, T. Assimes, and S. Horvath. 2017. Epigenetic aging and immune senescence in women with insomnia symptoms: Findings from the women's health initiative study. *Biol. Psychiatr.* 81:136–144. https://doi.org/10.1016/j.biopsych.2016.07.008

Cedernaes, J., M. Schonke, J.O. Westholm, J. Mi, A. Chibalin, S. Voisin, M. Osler, H. Vogel, K. Hornaeus, S.L. Dickson, et al. 2018. Acute sleep loss results in tissue-specific alterations in genome-wide DNA methylation state and metabolic fuel utilization in humans. *Sci. Adv.* 4:eaar8590. https://doi.org/10.1126/sciadv.aar8590

Chen, Y.-C., P.Y. Hsu, C.C. Hsiao, and M.C. Lin. 2019. Epigenetics: A potential mechanism involved in the pathogenesis of various adverse consequences of obstructive sleep apnea. *Int. J. Mol. Sci.* 20:2937. https://doi.org/10.3390/ijms20122937

Dashti, H.S., I. Daghlas, J.M. Lane, Y. Huang, M.S. Udler, H. Wang, H.M. Ollila, S.E. Jones, J. Kim, A.R. Wood, et al. 2021. Genetic determinants of daytime napping and effects on cardiometabolic health. *Nat. Commun.* 12:900. https://doi.org/10.1038/s41467-020-20585-3

Depner, C.M., E.L. Melanson, R.H. Eckel, J.K. Snell-Bergeon, L. Perreault, B.C. Bergman, J.A. Higgins, M.K. Guerin, E.R. Stothard, S.J. Morton, and K.P. Wright Jr. 2019. Ad libitum weekend recovery sleep fails to prevent metabolic dysregulation during a repeating pattern of insufficient sleep and weekend recovery sleep. *Curr. Biol.* 29:957–967.e4. https://doi.org/10.1016/j.cub.2019.01.069

Dimitrov, S., T. Lange, S. Tieken, H.L. Fehm, and J. Born. 2004. Sleep associated regulation of T helper 1/T helper 2 cytokine balance in humans. *Brain Behav. Immun.* 18:341–348. https://doi.org/10.1016/j.bbi.2003.08.004

Dimitrov, S., T. Lange, C. Benedict, M.A. Nowell, S.A. Jones, J. Scheller, S. Rose-John, and J. Born. 2006. Sleep enhances IL-6 trans-signaling in humans. *FASEB J.* 20:2174–2176. https://doi.org/10.1096/fj.06-5754fje

Divangahi, M., P. Aaby, S.A. Khader, L.B. Barreiro, S. Bekkering, T. Chavakis, R. van Crevel, N. Curtis, A.R. DiNardo, J. Dominguez-Andres, et al. 2021. Trained immunity, tolerance, priming and differentiation: Distinct immunological processes. *Nat. Immunol.* 22:2–6. https://doi.org/10.1038/s41590-020-00845-6

Dorshkind, K., T. Hofer, E. Montecino-Rodriguez, P.D. Pioli, and H.R. Rodewald. 2020. Do haematopoietic stem cells age?. *Nat. Rev. Immunol.* 20:196–202. https://doi.org/10.1038/s41577-019-0236-2

Durrett, R. 2012. Essentials of Stochastic Processes. 2nd edition. Springer-Verlag, New York. https://doi.org/10.1007/978-1-4614-3615-7

Ewens, W.J. 2004. Mathematical Population Genetics 1. 2nd edition. Springer-Verlag, New York. https://doi.org/10.1007/978-0-387-21822-9

Ferguson, T., R. Curtis, F. Fraysse, R. Lagiseti, C. Northcott, R. Virgara, A. Watson, and C.A. Maher. 2021. Annual, seasonal, cultural and vacation patterns in sleep, sedentary behaviour and physical activity: A systematic review and meta-analysis. *BMC Publ. Health.* 21:1384. https://doi.org/10.1186/s12889-021-11298-3

Ford, E.S., T.J. Cunningham, and J.B. Croft. 2015. Trends in self-reported sleep duration among US adults from 1985 to 2012. *Sleep*. 38:829–832. https://doi.org/10.5665/sleep.4684

Friedman, E.M., M.S. Hayney, G.D. Love, H.L. Urry, M.A. Rosenkranz, R.J. Davidson, B.H. Singer, and C.D. Ryff. 2005. Social relationships, sleep quality, and interleukin-6 in aging women. *Proc. Natl. Acad. Sci. USA.* 102:18757–18762. https://doi.org/10.1073/pnas.0509281102

Full, K.M., J. Kerr, M.A. Grandner, A. Malhotra, K. Moran, S. Godoble, L. Natarajan, and X. Soler. 2018. Validation of a physical activity accelerometer device worn on the hip and wrist against polysomnography. *Sleep Health*. 4:209–216. https://doi.org/10.1016/j.sleh.2017.12.007

Genovese, G., A.K. Kahler, R.E. Handsaker, J. Lindberg, S.A. Rose, S.F. Bakhoum, K. Chambert, E. Mick, B.M. Neale, M. Fromer, et al. 2014. Clonal hematopoiesis and blood-cancer risk inferred from blood DNA sequence. *N. Engl. J. Med.* 371:2477–2487. https://doi.org/10.1056/nejmoa1409405

Geovanini, G.R., R. Wang, J. Weng, R. Tracy, N.S. Jenny, A.L. Goldberger, M.D. Costa, Y. Liu, P. Libby, and S. Redline. 2018. Elevations in neutrophils with obstructive sleep apnea: The Multi-Ethnic Study of Atherosclerosis (MESA). *Int. J. Cardiol.* 257:318–323. https://doi.org/10.1016/j.ijcard.2017.10.121

Heyde, A., D. Rohde, C.S. McAlpine, S. Zhang, F.F. Hoyer, J.M. Gerold, D. Cheek, Y. Iwamoto, M.J. Schloss, K. Vandoorne, et al. 2021. Increased stem cell proliferation in atherosclerosis accelerates clonal hematopoiesis. *Cell*. 184:1348–1361.e22. https://doi.org/10.1016/j.cell.2021.01.049

Hong, S., P.J. Mills, J.S. Loredo, K.A. Adler, and J.E. Dimsdale. 2005. The association between interleukin-6, sleep, and demographic characteristics. *Brain Behav. Immun.* 19:165–172. https://doi.org/10.1016/j.bbi.2004.07.008

Horne, J.A., and O. Ostberg. 1976. A self assessment questionnaire to determine Morningness Eveningness in human circadian rhythms. *Int. J. Chronobiol.* 4:97–110

Irwin, M.R. 2019. Sleep and inflammation: Partners in sickness and in health. *Nat. Rev. Immunol.* 19:702–715. https://doi.org/10.1038/s41577-019-0190-z

Jaiswal, S., P. Fontanillas, J. Flannick, A. Manning, P.V. Grauman, B.G. Mar, R.C. Lindsley, C.H. Mermel, N. Burtt, A. Chavez, et al. 2014. Age-related clonal hematopoiesis associated with adverse outcomes. *N. Engl. J. Med.* 371:2488–2498. https://doi.org/10.1056/nejmoa1408617

Jaiswal, S., P. Natarajan, A.J. Silver, C.J. Gibson, A.G. Bick, E. Shvartz, M. McConkey, N. Gupta, S. Gabriel, D. Ardissino, et al. 2017. Clonal hematopoiesis and risk of atherosclerotic cardiovascular disease. *N. Engl. J. Med.* 377:111–121. https://doi.org/10.1056/nejmoa1701719

Johns, M.W. 1991. A new method for measuring daytime sleepiness: The Epworth sleepiness scale. *Sleep*. 14:540–545. https://doi.org/10.1093/sleep/14.6.540

Kamel, N.S., and J.K. Gammack. 2006. Insomnia in the elderly: Cause, approach, and treatment. *Am. J. Med.* 119:463–469. https://doi.org/10.1016/j.amjmed.2005.10.051

Khan, N., J. Downey, J. Sanz, E. Kaufmann, B. Blankenhaus, A. Pacis, E. Pernet, E. Ahmed, S. Cardoso, A. Nijnik, et al. 2020. M. tuberculosis reprograms hematopoietic stem cells to limit myelopoiesis and impair trained immunity. *Cell.* 183:752–770.e22. https://doi.org/10.1016/j.cell.2020.09.062

Lallukka, T., L. Sares-Jaske, E. Kronholm, K. Saaksjarvi, A. Lundqvist, T. Partonen, O. Rahkonen, and P. Knekt. 2012. Sociodemographic and socioeconomic differences in sleep duration and insomnia-related symptoms in Finnish adults. *BMC Publ. Health.* 12:565. https://doi.org/10.1186/1471-2458-12-565

Lange, T., S. Dimitrov, H.L. Fehm, J. Westermann, and J. Born. 2006. Shift of monocyte function toward cellular immunity during sleep. *Arch. Intern. Med.* 166:1695–1700. https://doi.org/10.1001/archinte.166.16.1695

Langer, G., and C. Filer. 2020. 2020 sleep in America poll – sleepiness. *Sleep Health.* 6:e1–e3.

Leger, D., J.B. Richard, O. Collin, F. Sauvet, and B. Faraut. 2020. Napping and weekend catchup sleep do not fully compensate for high rates of sleep debt and short sleep at a population level (in a representative nationwide sample of 12, 637 adults). *Sleep Med.* 74:278–288. https://doi.org/10.1016/j.sleep.2020.05.030

Li, X., R. Joehanes, I. Hoeschele, S.S. Rich, J.I. Rotter, D. Levy, Y. Liu, S. Redline, and T. Sofer. 2019. Association between sleep disordered breathing and epigenetic age acceleration: Evidence from the Multi-Ethnic Study of Atherosclerosis. *EBioMedicine.* 50:387–394. https://doi.org/10.1016/j.ebiom.2019.11.020

Libby, P., and V.Z. Rocha. 2018. All roads lead to IL-6: A central hub of cardiometabolic signaling. *Int. J. Cardiol.* 259:213–215. https://doi.org/10.1016/j.ijcard.2018.02.062

McAlpine, C.S., M.G. Kiss, S. Rattik, S. He, A. Vassalli, C. Valet, A. Anzai, C.T. Chan, J.E. Mindur, F. Kahles, et al. 2019. Sleep modulates haematopoiesis and protects against atherosclerosis. *Nature.* 566:383–387. https://doi.org/10.1038/s41586-019-0948-2

Mindur, J.E., and F.K. Swirski. 2019. Growth factors as immunotherapeutic targets in cardiovascular disease. *Arterioscler. Thromb. Vasc. Biol.* 39:1275–1287. https://doi.org/10.1161/ATVBAHA.119.311994

Mitchell, E., M. Spencer Chapman, N. Williams, K.J. Dawson, N. Mende, E.F. Calderbank, H. Jung, T. Mitchell, T.H.H. Coorens, D.H. Spencer, et al. 2022. Clonal dynamics of haematopoiesis across the human lifespan. *Nature.* 606:343–350. https://doi.org/10.1038/s41586-022-04786-y

Morrison, S.J., A.M. Wandycz, K. Akashi, A. Globerson, and I.L. Weissman. 1996. The aging of hematopoietic stem cells. *Nat. Med.* 2:1011–1016. https://doi.org/10.1038/nm0996-1011

Nachun, D., A.T. Lu, A.G. Bick, P. Natarajan, J. Weinstock, M.D. Szeto, S. Kathiresan, G. Abecasis, K.D. Taylor, X. Guo, et al. 2021. Clonal hematopoiesis associated with epigenetic aging and clinical outcomes. *Aging Cell.* 20:e13366. https://doi.org/10.1111/acel.13366

Netzer, N.C., R.A. Stoohs, C.M. Netzer, K. Clark, and K.P. Strohl. 1999. Using the Berlin questionnaire to identify patients at risk for the sleep apnea syndrome. *Ann. Intern. Med.* 131:485–491. https://doi.org/10.7326/0003-4819-131-7-199910050-00002

Nicodeme, E., K.L. Jeffrey, U. Schaefer, S. Beinke, S. Dewell, C.W. Chung, .R Chandwani, I. Marazzi, P. Wilson, H. Coste, et al. 2010. Suppression of inflammation by a synthetic histone mimic. *Nature.* 468:1119–1123. https://doi.org/10.1038/nature09589

Ohayon, M.M., M.A. Carskadon, C. Guilleminault, and M.V. Vitiello. 2004. Meta-analysis of quantitative sleep parameters from childhood to old age in healthy individuals: Developing normative sleep values across the human lifespan. *Sleep.* 27:1255–1273. https://doi.org/10.1093/sleep/27.7.1255

Pietras, E.M., D. Reynaud, Y.A. Kang, D. Carlin, F.J. Calero-Nieto, A.D. Leavitt, J.M. Stuart, B. Gottgens, and E. Passegue. 2015. Functionally distinct subsets of lineage-biased multipotent progenitors control blood production in normal and regenerative conditions. *Cell Stem Cell.* 17:35–46. https://doi.org/10.1016/j.stem.2015.05.003

Poon, G.Y.P., C.J. Watson, D.S. Fisher, and J.R. Blundell. 2021. Synonymous mutations reveal genome-wide levels of positive selection in healthy tissues. *Nat. Genet.* 53:1597–1605. https://doi.org/10.1038/s41588-021-00957-1

Ridker, P.M., and M. Rane. 2021. Interleukin-6 signaling and anti-interleukin-6 therapeutics in cardiovascular disease. *Circ. Res.* 128:1728–1746. https://doi.org/10.1161/CIRCRESAHA.121.319077

Rodrigues, C.P., M. Shvedunova, and A. Akhtar. 2021. Epigenetic regulators as the gatekeepers of hematopoiesis. *Trends Genet.* 37:125–142. https://doi.org/10.1016/j.tig.2020.09.015

Rossi, D.J., D.Bryder, J.M.Zahn, H.Ahlenius, R.Sonu, A.J.Wagers, and I.L.Weissman. 2005. Cell Intrinsic alterations underlie hematopoietic stem cell aging. *Proc. Natl. Acad. Sci. USA.* 102:9194–9199. https://doi.org/10.1073/pnas.0503280102

Ruiz, F.S., M.L. Andersen, R.C. Martins, A. Zager, J.D. Lopes, and S. Tufik. 2012. Immune alterations after selective rapid eye movement or total sleep deprivation in healthy male volunteers. *Innate Immun.* 18:44–54. https://doi.org/10.1177/1753425910385962

Samanta, A., B. Li, X. Song, K. Bembas, G. Zhang, M. Katsumata, S.J. Saouaf, Q. Wang, W.W. Hancock, Y. Shen, and M.I. Greene. 2008. TGF-beta and IL-6 signals modulate chromatin binding and promoter occupancy by acetylated FOXP3. *Proc. Natl. Acad. Sci. USA.* 105:14023–14027. https://doi.org/10.1073/pnas.0806726105

Shen, W., M. Punyanitya, Z. Wang, D. Gallagher, M.P. St-Onge, J. Albu, S.B. Heymsfield, and S. Heshka. 2004. Visceral adipose tissue: Relations between single-slice areas and total volume. *Am. J. Clin. Nutr.* 80:271–278. https://doi.org/10.1093/ajcn/80.2.271

Shen, Y.J., Y. Mishima, J. Shi, R. Sklavenitis-Pistofidis, R.A. Redd, M. Moschetta, S. Manier, A.M. Roccaro, A. Sacco, Y.T. Tai, et al. 2021. Progression signature underlies clonal evolution and dissemination of multiple myeloma. *Blood.* 137:2360–2372. https://doi.org/10.1182/blood.2020005885

Snippert, H.J., L.G. van der Flier, T. Sato, J.H. van Es, M. van den Born, C. Kroon-Veenboer, N .Barker, A.M. Klein, J. van Rheenen, B.D. Simons, and H. Clevers. 2010. Intestinal crypt homeostasis results from neutral competition between symmetrically dividing Lgr5 stem cells. *Cell.* 143:134–144. https://doi.org/10.1016/j.cell.2010.09.016

Unruh, M.L., S. Redline, M.W. An, D.J. Buysse, F.J. Nieto, J.L. Yeh, and A.B. Newman. 2008. Subjective and objective sleep quality and aging in the sleep heart health study. *J. Am. Geriatr. Soc.* 56:1218–1227. https://doi.org/10.1111/j.1532-5415.2008.01755.x

Vallat, R., V.D. Shah, S. Redline, P. Attia, and M.P. Walker. 2020. Broken sleep predicts hardened blood vessels. *PLoS Biol.* 18:e3000726. https://doi.org/10.1371/journal.pbio.3000726

Consensus Conference Panel, Watson, N.F., M.S.Badr, G. Belenky, D.L. Bliwise, O.M. Buxton, D. Buysse, D.F. Dinges, J. Gangwisch, M.A. Grandner, et al. 2015. Joint consensus statement of the American academy of sleep medicine and sleep research society on the recommended amount of sleep for a healthy adult: Methodology and discussion. *J. Clin. Sleep Med.* 11:931–952. https://doi.org/10.5664/jcsm.4950

Weber, G.F., B.G. Chousterman, S. He, A.M. Fenn, M. Nairz, A. Anzai, T. Brenner, F. Uhle, Y. Iwamoto, C.S. Robbins, et al. 2015. Interleukin-3 amplifies acute inflammation and is a potential therapeutic target in sepsis. *Science.* 347:1260–1265. https://doi.org/10.1126/science.aaa4268

Yu, V.W.C., R.Z. Yusuf, T. Oki, J. Wu, B. Saez, X. Wang, C. Cook, N. Baryawno, M.J. Ziller, E. Lee, et al. 2016. Epigenetic memory underlies cell-autonomous heterogeneous behavior of hematopoietic stem cells. *Cell.* 167:1310–1322.e17. https://doi.org/10.1016/j.cell.2016.10.045

Zink, F., S.N. Stacey, G.L. Norddahl, M.L. Frigge, O.T. Magnusson, I. Jonsdottir, T.E. Thorgeirsson, A. Sigurdsson, S.A. Gudjonsson, J. Gudmundsson, et al. 2017. Clonal hematopoiesis, with and without candidate driver mutations, is common in the elderly. *Blood.* 130:742–752. https://doi.org/10.1182/blood-2017-02-769869

Supplemental material

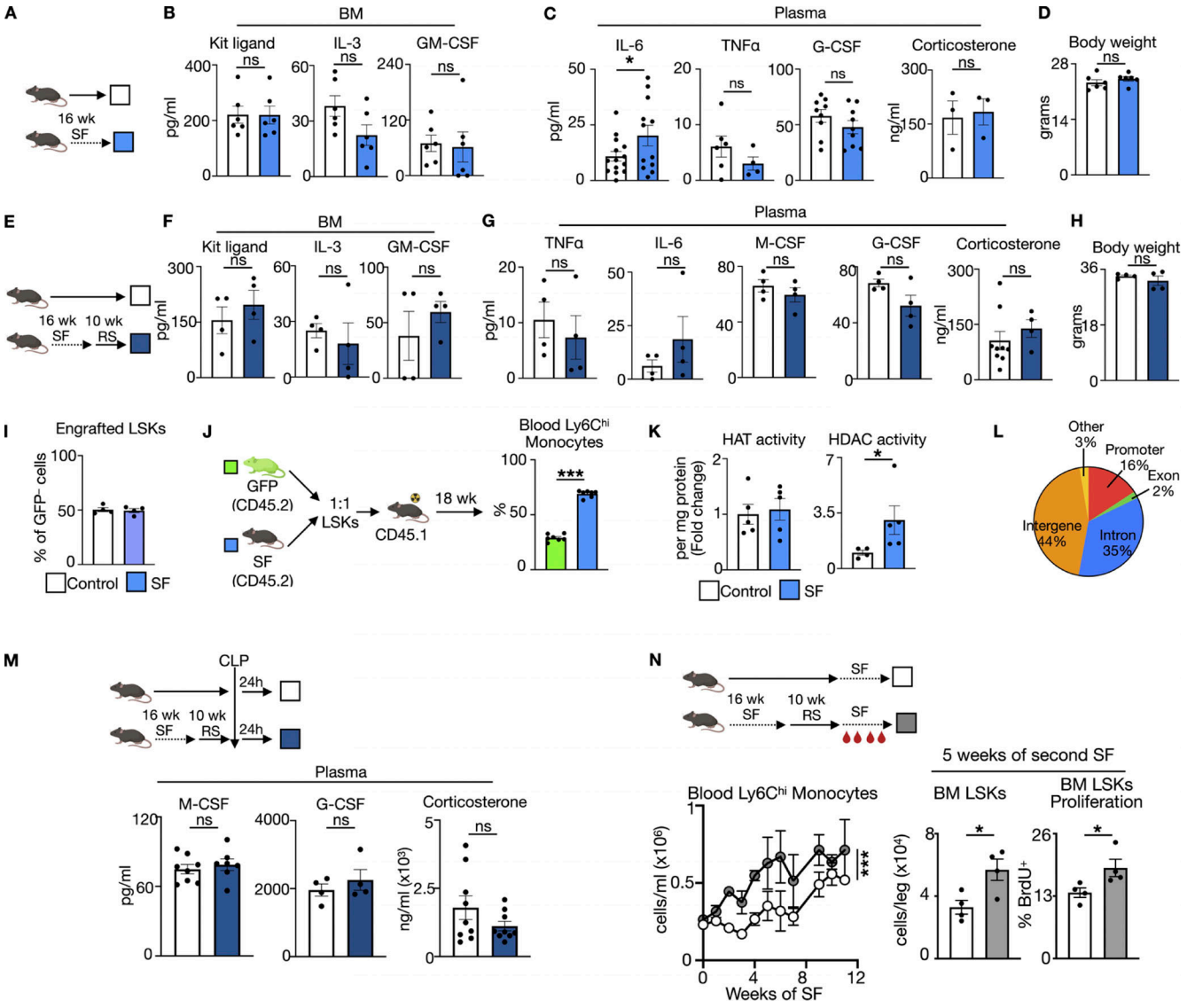

Figure S1. **Influence of SF and RS on inflammation, LSK fitness, epigenetic rewiring, and adaptability. (A)** Experimental design. **(B)** Growth factor levels in the BM fluid. **(C)** Cytokine, growth factor, and corticosterone levels in plasma of control and SF mice (n = 3–14 mice per group). **(D)** Body weight measurement of control and SF mice. **(E)** Experimental schematic of control mice and mice exposed to 16 wk of SF followed by 10 wk of RS. **(F)** Growth factor levels in the BM fluid. **(G)** Levels of plasma cytokines, growth factors, and corticosterone (n = 4 mice per group). **(H)** Body weight of control and SF+RS mice (n = 4 mice per group). **(I)** Engraftment of control GFP⁻CD45.1 and SF GFP⁻CD45.2 LSKs in the BM 24 h after transplantation. **(J)** Competitive 1:1 transplantation of LSKs from control (GFP⁺CD45.2) or SF (GFP⁻CD45.2) mice into a CD45.1 recipient mice and quantification of GFP⁺ vs. GFP⁻ chimerism among blood Ly6C^{hi} monocytes 18 wk after transplantation. n = 7 mice per group. **(K)** HAT and HDAC activity in BM lineage⁻cKit⁺ cells. n = 4–5 mice per group. **(L)** Genomic distribution of accessibility peaks in LSK ATAC-seq data. **(M)** Analysis of hematopoietic growth factors and corticosterone levels in plasma of control and SF+RS mice after CLP (n = 4–8 mice per group). **(N)** Schematic of repeated SF episodes. Blood monocytosis during first or second SF exposure (n = 5 mice per group) and BM LSKs and proliferation 5 wk after initiating first or second SF exposure (n = 4 mice per group). Mean ± SEM. *, P < 0.05; ***, P < 0.001.

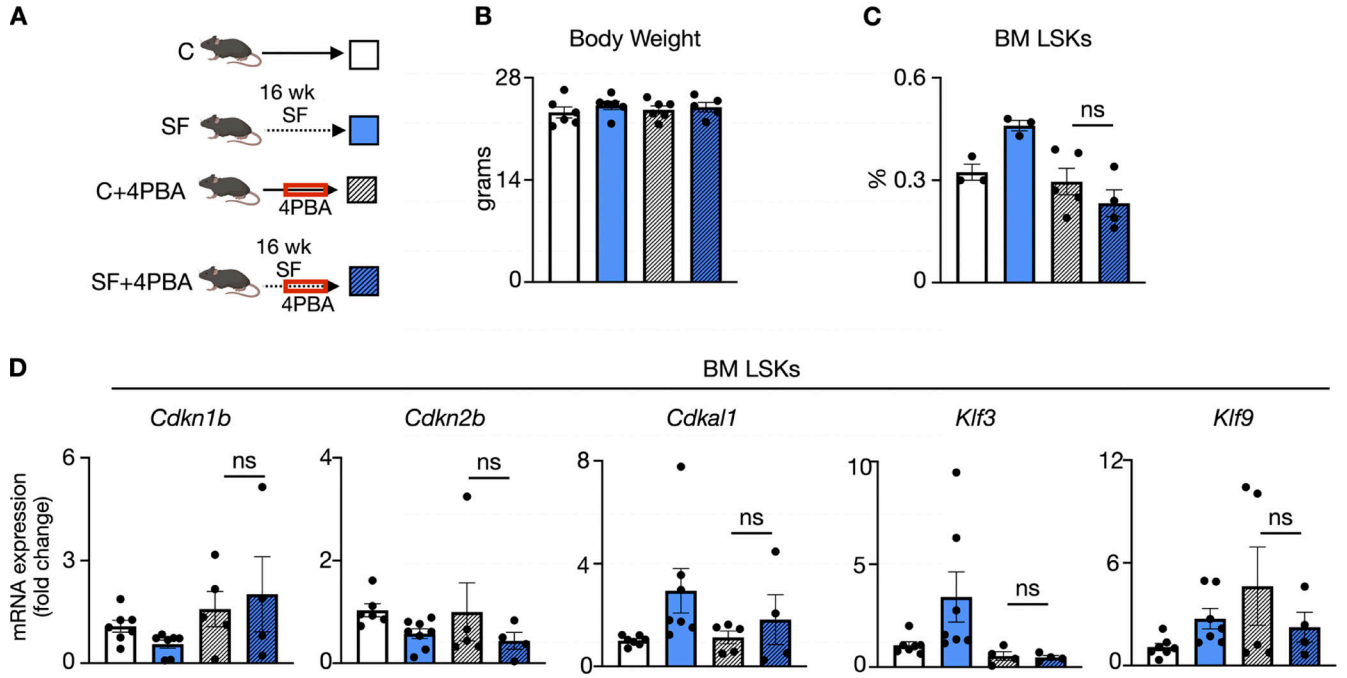

Figure S2. **Analysis of mice treated with 4PBA. (A)** Experimental design of 4PBA treatment during weeks 8 through 16 of control (C) sleep or SF. **(B)** Body weight, data of C and SF mice are as in Fig. S1 (*n* = 5–6 mice per group). **(C)** Proportion of BM LSKs (*n* = 3–5 mice per group). **(D)** Expression of *Cdkn1b*, *Cdkn2b*, *Cdkal1*, *Klf3*, and *Klf9* genes in sorted LSKs; data from control and SF mice are as in Fig. 2 G (*n* = 4–7 mice per group).

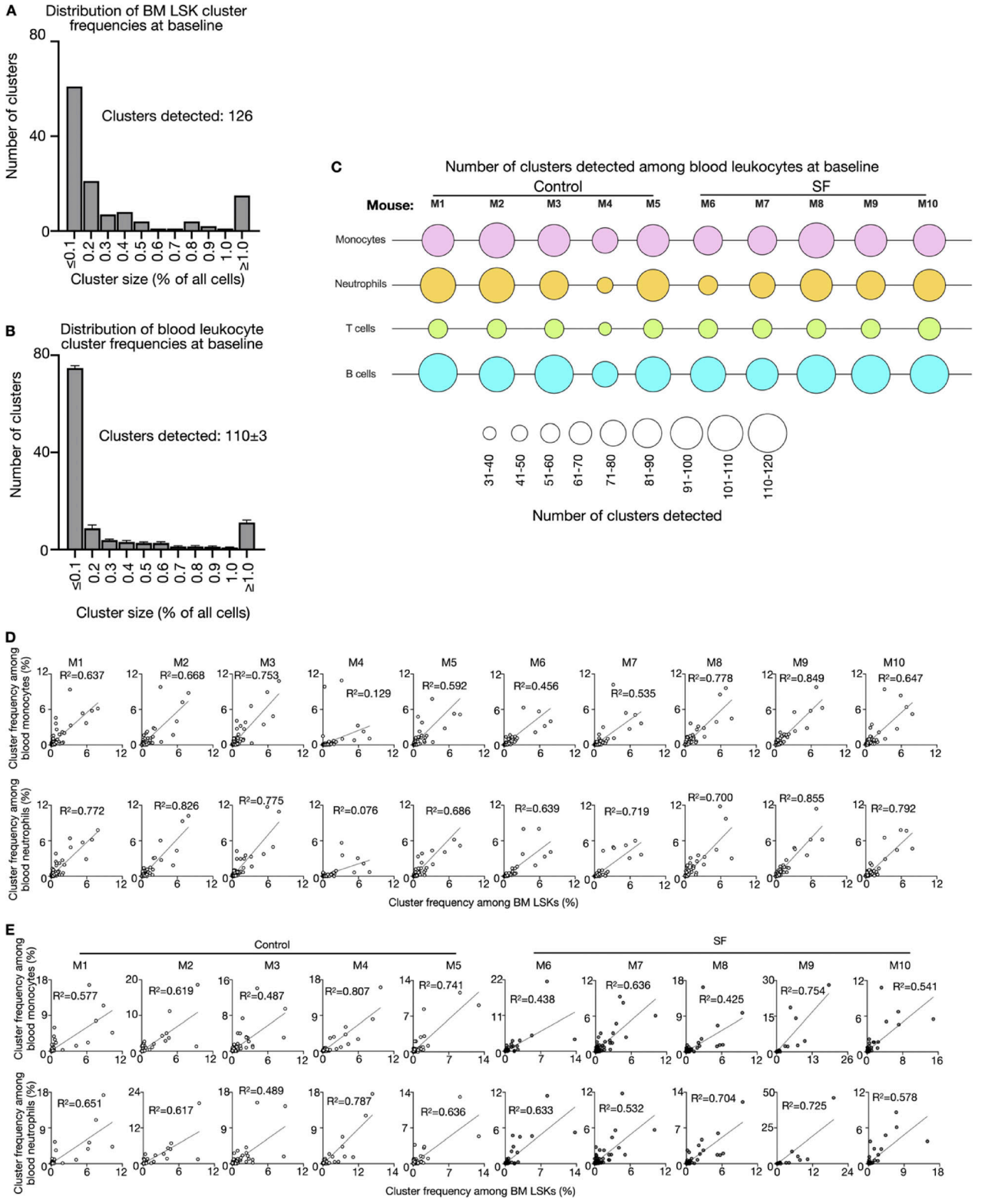

Figure S3. **Cluster size and distribution and correlation of cluster frequencies in the BM and blood. (A and B)** Distribution of tagged cluster frequency among LSKs (A) and blood leukocytes (B) at baseline. **(C)** Number of clusters detected at baseline among blood monocytes, neutrophils, T cells, and B cells. **(D and E)** Correlation of cluster frequency between BM LSKs and blood monocytes, and BM LSKs and blood neutrophils in each mouse at baseline (D; correlating transplanted LSKs with blood cells 6 wk after transplantation, prior to starting SF) and after 18 wk of SF or HS (E). *n* = 5 mice per group. M, mouse.

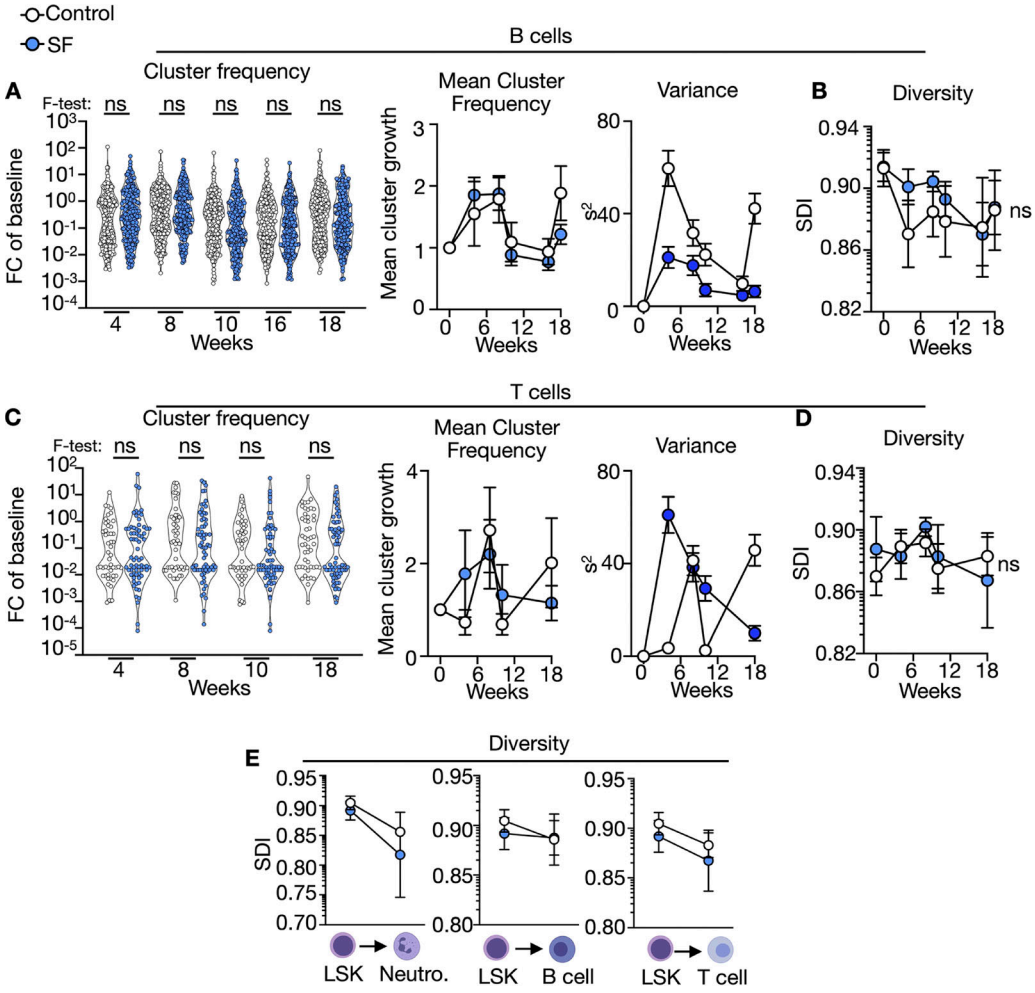

Figure S4. **Influence of sleep on lymphocyte diversity. (A)** Change in cluster frequency, mean cluster frequency, and variance of detectable B cell clusters with four or more tags. **(B)** SDI of B cells. **(C)** Change in cluster frequency, mean cluster frequency, and variance of detectable T cell clusters with four or more tags. **(D)** SDI of T cells. *n* = 5 mice per group. **(E)** Change in SDI from BM LSKs to blood neutrophils, B cells, and T cells. *n* = 5 mice per group. Mean ± SEM.

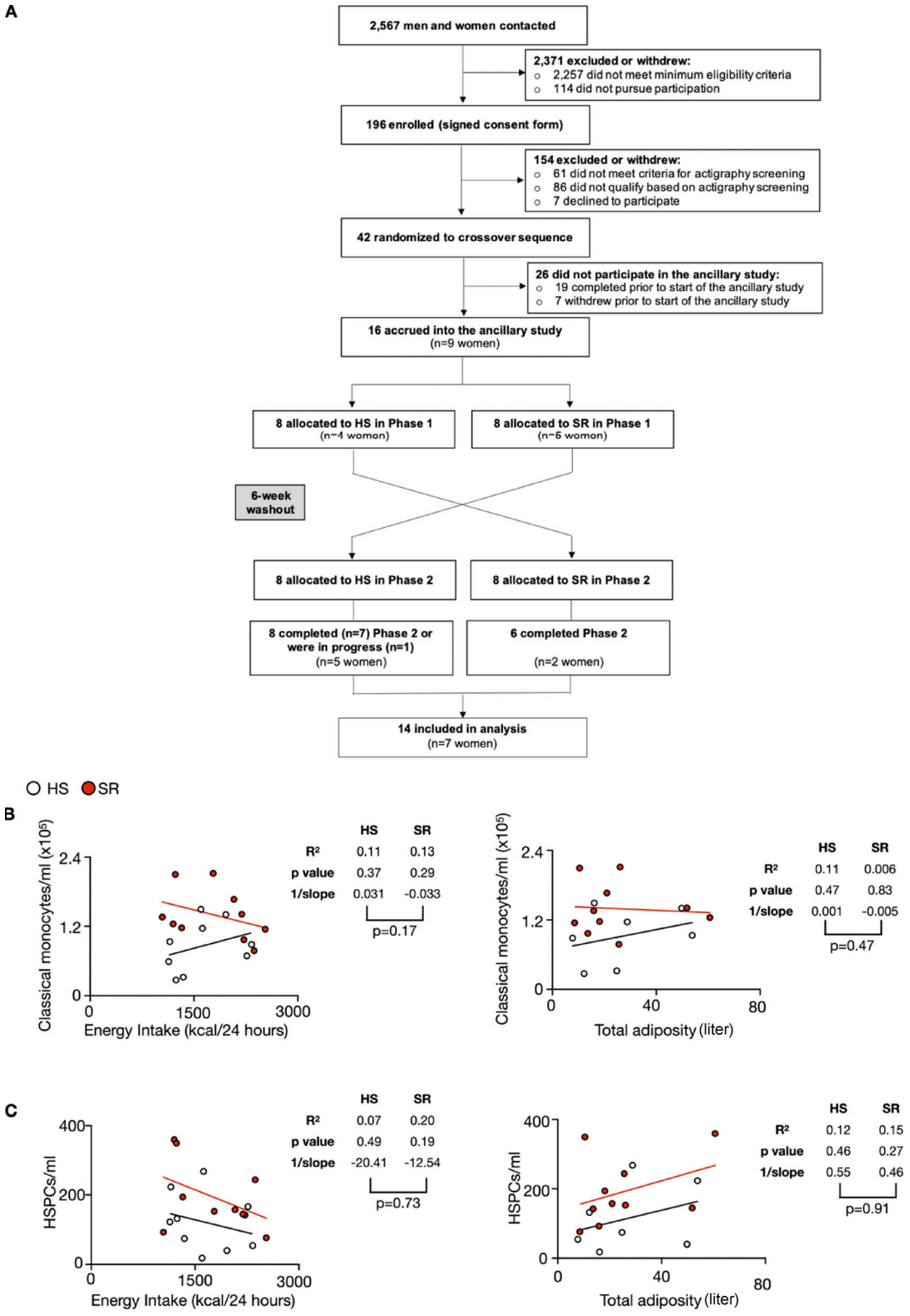

Figure S5. **Human study. (A–C)** Flow chart of the human study. Correlation of evening blood monocytes (B) and HSPCs (C) with energy intake and total adiposity at the completion of the HS and SR phases in human subject in which these parameters were available.

Provided online are three tables. Table S1 provides LSK cluster frequency. Table S2 lists number of LSKs in recipient control and SF mice. Fluorescent tagging recipient mice. Table S3 provides human subject characteristics at baseline.